

Orbits of small angular scale binaries resolved with the Mark III interferometer

C.A. HUMMEL¹, J.T. ARMSTRONG², D.F. BUSCHER³,
D. MOZURKEWICH² A. QUIRRENBACH⁴, and M. VIVEKANAND⁵

NRL/USNO Optical Interferometer Project

U.S. Naval Observatory, 3450 Massachusetts Avenue NW, Washington, DC 20392

Electronic mail: [cah,tarmstr]@fornax.usno.navy.mil, David.Buscher@durham.ac.uk,

mozurk@rira.nrl.navy.mil, quirrenbach@mpe-garching.mpg.de,

vivek@gmrt.ernet.in

Received _____; accepted _____

To be submitted to the Astronomical Journal

¹Universities Space Research Association, 300 D Street SW, Suite 801, Washington, DC 20024

²Remote Sensing Division, Naval Research Laboratory, Code 7215, Washington, DC 20375

³Department of Physics, University of Durham, South Road, Durham DH1 3LE, UK

⁴Max-Planck-Institut für extraterrestrische Physik, Giessenbachstraße, 85748 Garching, Germany

⁵National Center for Radio Astrophysics, Tata Institute of Fundamental Research, Pune University Campus, Post Bag 3, Ganeshkhind, Pune 411007, India

ABSTRACT

We present relative orbits of eight spectroscopic binaries with semimajor axes ranging from 3 milliarcseconds (mas) to 10 mas. The stars, π Andromedae, θ Aquilae, β Aurigae, ζ^1 Ursae Majoris, 93 Leonis, 113 Herculis, β Trianguli and δ Trianguli, represent some of the smallest angular scale binaries resolved with the Mark III optical interferometer on Mt. Wilson, California. In addition to the orbital elements, we measured the magnitude difference between the components at $\lambda\lambda$ 800 nm, 550 nm, 500 nm, and 450 nm. Spectroscopic orbital elements for both primary and secondary component are available for all stars except 113 Herculis. The available data allow the determination of the distance to four of the binaries, as well as of their component masses and luminosities. The results are compared with stellar evolution models.

1. Introduction

The study of spectroscopic binaries towards the determination of stellar masses, radii, colors, and luminosities has received significant impetus in recent years from observations with long-baseline interferometers, which have resolved more than two dozen of these stars, some of them at separations inaccessible to any other technique. In this paper, we present the visual orbits of eight binaries with semimajor axes less than about 10 milliarcseconds (mas). These observations were made with the Mark III interferometer⁶ whose resolution limit is about 3 mas at 450 nm on the longest baseline (31 m).

⁶The Mark III long-baseline optical interferometer, located on Mt. Wilson near Los Angeles, California, is operated by the Remote Sensing Division of the Naval Research Laboratory (NRL) with funding from the Office of Naval Research.

The observing program of spectroscopic binaries selected from the catalogue by was initiated in 1989, and a recent status report can be found in . In the course of this program, it has been demonstrated that high precision measurements of the orbital elements of binaries, as well as of the magnitude differences of the components and their diameters (if larger than about 3 mas) could be obtained with this instrument, providing valuable information to stellar astrophysical research.

2. Observations and data reduction

The Mark III long-baseline Michelson interferometer was described by . Two siderostats are operated at a time, and the two beams are combined at a beamsplitter after the geometrical delay has been compensated for in optical delay lines. The Mark III measures the stellar fringe contrast (i.e. the amplitude of the complex visibility) simultaneously in three different bands, centered at λ 800 nm, 550 nm, and 500 nm (450 nm in 1989), each about 25 nm in width. By means of earth rotation aperture synthesis, the amplitude of the two-dimensional visibility function (the complex visibility is the Fourier transform of the brightness distribution of the astronomical object) is sampled in the aperture plane. We obtain spatial information on the object by fitting models consisting of uniform or limb-darkened disks to the visibility data accumulated in one or more nights on various baselines (see for further information).

Raw visibility amplitudes are degraded by atmospheric turbulence (characterized by the seeing index) and instrumental effects such as alignment and quality of the optical elements. To separate these effects from the contribution due to stellar structure, calibrator stars with small angular size (less than 2 mas), and thus whose visibilities are nearly that of a point source (i.e. constant with baseline length and orientation), are used to normalize the visibilities of the program stars. This procedure was described in detail by . Calibration

uncertainties are typically a few percent for the red channel and up to 15 percent for the blue channel.

In a typical night, a total of some 100 to 200 scans of 75 s on-source duration were obtained on the N-S baseline, which was configured to lengths ranging from 3 m to 31 m. These scans were distributed over a list of 5 to 15 stars, half of them calibrators which were chosen to be close to the program stars.

3. Derivation of orbital elements and component parameters

The seven orbital elements are the semimajor axis a in mas, eccentricity e , period P , epoch of periastron passage T , inclination i , position angle of the ascending node Ω , and the argument of the periastron ω . Component parameters are the diameters D_1 and D_2 at 800 nm and the magnitude differences $\Delta m(\lambda)$ of the components at $\lambda\lambda$ 800 nm, 550 nm, and 450 nm (approximately corresponding to bands I_C , V , and B , respectively). Component diameters at $\lambda\lambda$ 550 nm and 450 nm are adopted as 95 percent of the diameter at 800 nm to account for limb darkening. Since all component diameters reported in this paper are only slightly resolved if not unresolved, this approximation is adequate. Values of the component parameters at other observed wavelengths (e.g. 500 nm) are interpolated by quadratic polynomials.

Initial estimates of the orbital elements were obtained by applying the Thiele-Innes method (see, e.g.,) to estimates of the position angle θ and separation ρ of the binary components derived from individual nights as described in . For the final elements and component parameters we used the method of of a fit directly to the measured visibilities. This global fit is the most efficient approach to constrain the component parameters if the components are not variable (none of the stars reported on in this paper are variable above

a level which would significantly affect our results). The method can also make use of data taken in nights with insufficient coverage to constrain a fit of ρ and θ , and is able to derive orbital elements when the orbital motion is too large to define ρ and θ uniquely for a single night.

Estimates for the uncertainty of the fit parameters were based on three methods, which generally produced consistent results. First, the diagonal elements of the covariance matrix provided formal uncertainties which were adopted as lower limits for the actual uncertainty estimates. Second, we performed Monte-Carlo simulations of artificial data with various error distribution models as described in . Uncertainty estimates were derived from the spread in the parameter values of models fitted to the artificial data sets. Third, an empirical estimate was derived from the variations of model parameters when new data had been obtained and added to the data base.

4. Results

In Table 1 we list the results for orbital elements and component parameters from the Mark III interferometer, as well as results for orbital elements from spectroscopy. References for the latter are included at the bottom of each column of the table. Subscripts M and S indicate Mark III and spectroscopic determinations, respectively. The epoch T is the epoch of periastron passage, except for β Aurigae and 93 Leonis, where it is the epoch of passage through the ascending node. An integer multiple of the period has been added to the epoch from spectroscopy to facilitate comparison with the epoch from the Mark III data. For the sake of an independent determination of the orbital elements, we did not adopt the high-precision spectroscopic value for the period (given in the table to all significant figures) but determined its value from the fit for stars with a sufficient amount of data. The two results, however, do agree very well and made a fit of our data with the

spectroscopic period seem unnecessary. We also include information in the table on the number of visibility measures used in the fit, the mean epoch, and the reduced χ^2 , χ^2_ν of the fit.

The orbits are shown in Figs. 1–8. In the figures, a small arrow indicates the sense of revolution, T denotes the periastron (with the straight solid line indicating the major axis), or T_0 denotes the ascending node (with the straight solid line indicating the line of nodes). Relative binary positions (ρ, θ) and corresponding uncertainty ellipses were derived from the data of each night in order to indicate the amount and quality of the data and their weights. The uncertainty ellipses were computed as follows: we adopted the diameters and magnitude differences from the global fit and determined values for ρ and θ from the data of each night. (We accounted for orbital motion during the nights using the rate of change for ρ and θ derived from the parameters of the global fit.) The visibility uncertainties were scaled to normalize the reduced χ^2 of the fit to unity, and uncertainty ellipses were fitted to the locus of (ρ, θ) values where the total χ^2 increased by one over its minimum value (i.e. the number of visibilities). Tables 2–9 list the results; cols. 1 and 2 give date and fractional Besselian year of the observation (at 8 UT), col. 3 the length of the baseline, col. 4 the number of scans, cols. 5 and 6 separation and position angle (equinox = mean epoch) at 8 UT, cols. 7 to 9 the axes and the position angle of the uncertainty ellipse, and col. 10 the deviation of the fitted relative binary position (ρ, θ) from the model values. Position angles are measured counterclockwise (over east) from north. We ask the reader to keep in mind that the orbital elements were not fitted to the listed binary positions, but to the visibilities as described in the last section.

The visibility amplitude of binaries varies quasi-sinusoidally with time on a given baseline (Armstrong 1992). Due to the small angular scale of the binaries in this work, the observations often do not cover more than one cycle of the variations. For this reason,

calibration errors generally have a larger influence on measured separations and position angles as compared to observations of wider binaries. In the cases of unidentified calibration errors, the fitted error ellipses therefore might drift off the orbit significantly as can be seen in the orbits for β Aurigae and ζ^1 Ursae Majoris. We believe that the global fitting algorithm described in the last section is more robust in such circumstances than an algorithm based on fitting separations and position angles.

5. Discussion

In the following, we will discuss each star individually. As our procedures for obtaining physical parameters from the observables are similar in each case, they will be described in somewhat more detail only on the example of θ Aquilae. In general, we focus on the determination of stellar masses, effective temperatures, and luminosities, which we compare to predictions by stellar evolution models for coeval components. As these models depend on the chemical composition of the stars, we adopt for lack of reliable measurements a metallicity which produces the best overall fit to the physical parameters. We usually assume effective temperatures according to the spectral types of the components, making sure that their colors are consistent with the temperatures.

5.1. π Andromedae

Orbital elements from spectroscopy listed for this star No. 31 (= 29 And = HR 154 = HD 3369 = SAO 54033 = ADS 513 A [companion 9^m0 at 36^{''}]) in the catalogue by were derived by . The elements of the primary are considered ‘definitive’ by B89, and those common to the set of visual elements agree quite well with our determinations. The combined spectrum of the components has been consistently classified over the years as

type B5V (e.g.). The small variation in magnitude difference with wavelength indicates that the two components are similar in spectral type. Pearce was the only one who observed the secondary spectrum: he determined $K_1 = 47.50 \pm 0.53$ km/s and $K_2 = 117.4 \pm 2.8$ km/s. and failed to measure K_2 , giving the relative weakness of the secondary spectrum as a reason. With Pearce’s values however, we derive stellar masses for the primary and secondary components of $29\mathcal{M}_\odot$ and $12\mathcal{M}_\odot$, respectively, much too large for a type B5V star, for which we would expect about $5\mathcal{M}_\odot$ (). We point out that $\mathcal{M}_{1,2} \sin^3 i$ themselves are already larger than the expected masses, and that our value for the orbital inclination leads to a correction of the spectroscopically determined $\mathcal{M} \sin^3 i$ of only about 8% and therefore could not be considered for an explanation of the large discrepancy between measured masses and theoretical estimates. Only super-giant components of type B5 would have masses in the range 10 to 20 \mathcal{M}_\odot , but there is no other evidence to support that classification. We think it to be more likely that the secondary spectrum was not as well defined in Pearce’s observations as to warrant a reliable determination of K_2 .

Adopting the latter interpretation, we are effectively left with a single lined binary with a measured mass function of

$$f(\mathcal{M})/\sin^3 i \equiv \mathcal{M}_2^3/(\mathcal{M}_1 + \mathcal{M}_2)^2 = 1.0385 \cdot 10^{-7} (1 - e^2)^{3/2} K_1^3 P / \sin^3 i \mathcal{M}_\odot = 0.98 \mathcal{M}_\odot,$$

where e is the orbital eccentricity, K is in km/s, and P is in days (B89). We have measured a V -magnitude difference, Δm_V , of 0^m4, which translates into a mass ratio of 0.82 for main sequence stars around class B5 using a cubic fit to the $M_V - \mathcal{M}$ data obtained from eclipsing binaries by . Thus we find that a pair of components with masses of $5.8\mathcal{M}_\odot$ and $4.8\mathcal{M}_\odot$ would be consistent with our measurements and with spectral classifications between B3V and B6V. New spectroscopic measurements are obviously required to settle this disconcerting issue.

5.2. θ Aquilae

Both line systems of another pair of B-type stars, No. 1211 (= 65 Aql = HR 7710 = HD 191692 = SAO 144150) in B89, were measured by who derived elements which are rated ‘definitive’ in B89. There is good agreement for those elements which were measured with the Mark III interferometer, indicating that despite the somewhat uneven phase coverage in the Mark III orbit, the value of the orbital inclination should be a reliable one. Cesco & Struve found the components to be of roughly the same type, and the most recent classification of the spectral type of θ Aquilae, B9.5III, done by , is in agreement with the results of most of the other authors. estimated $\Delta m_V = 1.3$.

Combining spectroscopic and visual elements, we derive the distance to θ Aquilae and the masses of the components. The orbital parallax of $\pi = 0''.013 \pm 0''.001$ is in agreement with the trigonometric parallax of $\pi = 0''.011 \pm 0''.006$ listed by . We use the distance modulus to convert the combined apparent magnitudes ($m_V = 3^m23$ and $m_B = 3^m15$ from) into absolute magnitudes. Absolute component magnitudes in the B and V bands are then calculated from the combined magnitudes with our measured magnitude differences at 550 nm and 450 nm, respectively. The $(B - V)$ colors of the components are found to be nearly identical and consistent with their spectral type (). We did not correct for reddening, since at 75 pc distance we expect a correction to $(B - V)$ of less than 0^m03 . We adopt a single effective temperature for both components based on the spectral type and use formulas given by to determine the bolometric correction BC . Thus, we consecutively obtain the bolometric luminosities and predicted stellar radii separately for each component. The angular diameters of the components of θ Aquilae corresponding to the predicted diameters are 0.59 mas and 0.30 mas for primary and secondary, respectively. They are in good agreement with the diameters (0.57 mas and 0.28 mas) derived from the $(R - I)$ color index (-0^m05 , taken from and assumed to be identical for both components) and the

apparent visual magnitudes m_V of the components using the calibration obtained by . Being significantly smaller than 1 mas, the diameters cannot be measured with the Mark III. The results are listed in Table 10.

The uncertainty in the derived stellar masses is dominated by the uncertainty in our measurement of the orbital inclination. The adopted uncertainty in the effective temperature is based on an uncertainty in the spectral class of about one-half subclass. The uncertainty in the bolometric correction reflects both the uncertainty of the effective temperature entering the formula of Gubochkin & Miroschnichenko and the consistency of this calibration with calibrations given by and .

Due to the relatively low precision of the masses (and the distance), a rigorous comparison of the derived astrophysical parameters with those predicted by various stellar evolution models have to await better interferometric data. We will nevertheless outline in the following what can be done with the present results. Stellar evolution models with new radiative opacities have been published by and for metallicities $Z = 0.001, 0.008, \text{ and } 0.020$. (The tables, as well as program to construct isochrones, were kindly made available to us by G. Meynet.) More recently, published large grids of theoretical isochrones for metallicities $Z = 0.0004, 0.004, 0.008, 0.02, \text{ and } 0.05$. Using the models of B94 (and interpolating isochrones locally if necessary using the gridpoints), we find a pair of two solar-metallicity stars of $\log(\text{age}/\text{yr}) = 8.30 \pm 0.05$ which fits the luminosities and temperatures very well. The model masses are $3.68M_\odot$ and $2.76M_\odot$, for primary and secondary, respectively. The more massive component has slightly evolved off the main sequence. The best-fit isochrone of S92 has an age of $\log(\text{age}/\text{yr}) = 8.32$ and model masses of $3.55M_\odot$ and $2.75M_\odot$. We show the B94 isochrone (solid line) in Fig. 9. Best-fit isochrones for metallicities $Z = 0.008$ ($\log(\text{age}/\text{yr}) = 8.45, 3.24M_\odot$ and $2.54M_\odot$) and $Z = 0.05$ ($\log(\text{age}/\text{yr}) = 8.16, 3.80M_\odot$ and $2.89M_\odot$) cannot be ruled out based on our data, but are of discernably lower quality, as

can be seen in Fig. 9.

5.3. β Aurigae

A considerable amount of information regarding spectroscopic elements, absolute dimensions and physical parameters has been obtained on this eclipsing binary, No. 366 (= 34 Aur = HR 2088 = HD 40183 = SAO 40750) in B89, from spectroscopic work by, e.g., and photometry of the shallow eclipse (depth 0^m1) by . From we learn that the spectra of the components are nearly identical; they have been consistently classified as of type A2V-IV (e.g.).

Observations of β Aurigae with the Mark III interferometer are challenging, as the maximum separation between the components is always smaller than about 3 mas and significant orbital motion occurs even in a single night due to the short orbital period of about 4 days. At a separation of 3 mas, observations on the longest baselines cover about half a wavelength of the sinusoidal visibility variation in one night.

We note that our measurement of the V -magnitude difference is consistent with the determination by . Due to a correlation between our determinations of the diameters and the magnitude differences and due to the former being slightly resolved, we had adopted in the fit the diameters derived by NJ94, converted to angular diameters using our determination of the parallax. We note further that the value derived by NJ94 for the orbital inclination ($i = 76^{\circ}.7 \pm 0^{\circ}.2$) is in much better agreement with our value than the determination ($i = 77^{\circ}.8 \pm 0^{\circ}.2$) by .

For β Aurigae, effective temperatures have been determined directly with the physical component diameters obtained from eclipse photometry and converted to angular diameters using the trigonometric parallax π_{trig} , and with the integrated bolometric flux (e.g. . The

accuracy of T_{eff} had been limited by the accuracy of π_{trig} , a limitation which can now be overcome by replacing $\pi_{\text{trig}} = 0''.044 \pm 0''.005$ (with our higher precision orbital parallax $\pi_{\text{orb}} = 0''.040 \pm 0''.001$). Using Smalley and Dworetzky’s bolometric fluxes of the components (the bolometric flux ratio assumed to correspond to an adopted magnitude difference of $0^{\text{m}}12$) and physical diameters from NJ94, we find nearly identical effective temperatures for both components of $T_{\text{eff}} = (9070 \pm 200)$ K. The temperature is in good agreement with a spectral type of A2V based on Flower’s (1977) calibration with an uncertainty of about one sub-class. Table 11 lists derived physical parameters based on the adoption of identical $(B - V)$ colors for primary and secondary ($\Delta m_{550} = \Delta m_{450} = 0^{\text{m}}2 \pm 0^{\text{m}}2$). The uncertainty quoted for $(B - V)$ is derived from the uncertainties in the magnitude differences. The $(B - V)$ color is consistent with the spectral classification. We did not correct for reddening, a correction which would be negligible because of the small distance to β Aurigae. The component diameters are consistent with the diameters derived from the $(R - I)$ color index and the apparent V -magnitude ($(R - I) = -0^{\text{m}}01$, giving $D_{1,2} = 1.0$ mas).

Finally, we are interested in evaluating the evolutionary state of the β Aurigae stars from a comparison with the models by S92, S93, and B94. A suitable isochrone can be found in B94 for $Z = 0.020$ and $\log(\text{age}/\text{yr}) = 8.65 \pm 0.03$, where a pair of slightly evolved main-sequence stars with the correct luminosities has masses of $2.44\mathcal{M}_{\odot}$ and $2.36\mathcal{M}_{\odot}$ for primary and secondary, respectively (Fig. 10). A best-fit isochrone of $\log(\text{age}/\text{yr}) = 8.67$ using data from S92 gives component masses of $2.41\mathcal{M}_{\odot}$ and $2.34\mathcal{M}_{\odot}$. The agreement of the two different models and the data is impressive.

5.4. ζ^1 Ursae Majoris

This system, No. 764 (= HR 5054 = HD 116656 = SAO 28737) in B89, is almost identical to β Aurigae with respect to the spectral classification, which is A2V. (ζ^1 Ursae

Majoris is listed as an Ap-star [A1VpSrSi] in .) The combined color of ζ^1 Ursae Majoris is $(B - V) = 0^m02$, very close to what we would expect for an A2V star (0^m05 ,). derived $\Delta m_V = 0^m03$. From this we conclude that the two components of ζ^1 Ursae Majoris must be nearly identical. The spectroscopic elements derived by are considered ‘definitive’ by B89 in view of the consistency of the elements with those derived by several other authors (e.g.). H. N. Russell (as quoted by) used the 20-foot interferometer on Mt. Wilson to derive a visual orbit and found $i = 60^\circ$.

ζ^1 Ursae Majoris ($m_V = 2^m27$) is the brighter component of A.D.S. 8891: the companion ζ^2 is 3^m95 at about $14''$. With the Mark III, both ζ^1 and ζ^2 contribute to the total photon count rate, whereas the fringe packets are usually well separated. Thus, the visibility is reduced by a factor that is approximately constant with time because the photons from ζ^2 are uncorrelated if ζ^1 is being tracked, creating a calibration error for the ζ Ursae Majoris data. An estimate f for the visibility reduction can be derived from the magnitude difference between ζ^1 and ζ^2 , $\Delta m_{2-1} = 1^m68$, and is $f = (10^{-\Delta m/2.5} + 1)^{-2} = 0.68$.

As calibration errors have a direct influence on diameters and magnitude differences (but much less so on orbital parameters), we adopted component diameters of 0.8 mas derived from the $(R - I)$ color index and the apparent visual magnitude following the procedure described by , and a magnitude difference of zero in all channels. We fitted orbital elements to the data, adjusting the calibration constants for each night and channel after each iteration of the least-squares fitting algorithm. The resulting calibration factors were independent of the baseline length and of the channel. The latter result is consistent with the fact that the $(B - V)$ color index of ζ^2 (0^m13) is close that of ζ^1 (0^m02). The average visibility reduction was about 0.67 ± 0.01 . No systematic trends are observed in any of the nights. Rather than try to remove the effect of the uncorrelated photons from the data, we decided to keep the adopted diameter and magnitude difference estimates, as

they seemed to be consistent with our data.

In Table 12 we list the physical parameters based on the assumption of identical components. We adopted an uncertainty in the magnitude differences of 0^m1 . Further, we adopted an effective temperature corresponding to a type A2 star (). The derived orbital parallax ($\pi = 0''.0383 \pm 0''.0004$) agrees with the trigonometric parallax ($\pi = 0''.041 \pm 0''.006$) listed in .

If we compare the physical parameters of ζ^1 Ursae Majoris to those of β Aurigae, we find that despite being of the same spectral type, the former star has components fainter by about 0^m3 yet more massive by about 10%. In order to approximate the observed luminosities, effective temperatures, and masses, we have to adopt a larger-than-solar metallicity. With $Z = 0.05$ and $\log(age/yr) = 8.38$, we get a good fit to L and T_{eff} , but with $\mathcal{M} = 2.36\mathcal{M}_{\odot}$, somewhat lower than the measured masses.

5.5. 93 Leonis

The first of two binaries in our list with a late type evolved component and an early type dwarf, No. 690 (= HR 4527 = HD 102509 = SAO 81998) in B89 is double-lined. A revised orbit from spectroscopy was last published by . Since the orbital eccentricity was found to be negligibly small by these authors and was consistent with being zero in our first solution, we adopted a circular orbit in the final solution. The amount of data obtained for this star with the Mark III is significantly smaller compared to that for the other stars presented here, so we adopted the value for the period from the spectroscopic orbit. For the same reason, we adopted a value (0^m7) for the $(B - V)$ color difference of the two components consistent with their spectral classes of G5III and A7V () for primary and secondary, respectively. Finally, the angular diameter of the dwarf was set to 0.3 mas (see

next paragraph; this diameter is practically unresolvable with the Mark III), whereas the diameter of the primary was a free parameter in the fit.

93 Leonis is very similar to α Equulei (spectral types G5III and A5V) which has been observed with the Mark III by . The combined color indices ($B - V$) and ($R - I$) are nearly identical for both stars (α Equulei: ($B - V$) = 0^m53 and ($R - I$) = 0^m35 ; 93 Leonis: ($B - V$) = 0^m55 and ($R - I$) = 0^m36). The component angular diameters we adopted for the secondary and measured for the primary are consistent with the values derived for α Equulei from the ($R - I$) color index and m_V by . estimated $\Delta m_V = 0^m43$ and estimated $\Delta m_B = -0^m36$, both estimates being consistent with our results and the results for α Equulei.

In Table 13, we summarize physical parameters derived for 93 Leonis. We adopted effective temperatures corresponding to the spectral types of the components according to , and uncertainties corresponding to an error in the classification of about one sub-class. The derived orbital parallax of $\pi = 0''.0138 \pm 0''.0005$ is in reasonable agreement with the trigonometric parallax of $\pi = 0''.021 \pm 0''.009$ in .

The masses and luminosities of the components of 93 Leonis are close to those of the corresponding components of α Equulei, once more underlining the similarity of these two systems. From a comparison with the models of B94 we find a slightly better fit with isochrones for stellar models of lower-than-solar metallicity ($Z = 0.008$). The evolutionary state at age $\log(\text{age}/\text{yr}) = 9.0$ is indicated in Fig. 11; the model stellar masses are $2.1\mathcal{M}_\odot$ and $1.9\mathcal{M}_\odot$ for primary and secondary, respectively, and are consistent with the measured masses. However, due to the uncertainties in L and T_{eff} , the solar-metallicity model (which produces masses somewhat closer to the measured ones) cannot be ruled out. Still, the observations do allow to distinguish between subtle differences of the isochrones of S93 and B94 due to the large separation in spectral type between the two components of 93 Leonis.

An alternative isochrone from S93 for same the metallicity and age as the B94-isochrone is plotted in Fig. 11. Clearly, the B94 model is a better fit to the data.

5.6. 113 Hercules

Not much can be added here to our knowledge in terms of basic physical parameters of this star, No. 1100 (= HR 7133 = HD 175492 = SAO 86567) in B89, because the radial velocity of only the later-type has been measured (,). 113 Hercules consists of two stars of type G4III and A6V. derived an angular diameter of 1.4 mas and an effective temperature of 5200 K for an assumed single star using the infrared flux method. With our measured magnitude difference and bolometric corrections listed for the spectral types in , we estimate that the bolometric flux of the giant component is the larger of the two by about 2^m . Since, in addition, the A6 star contributes only a negligible amount of flux in the infrared, we conclude that the derived diameter must approximate that of the giant component. This is supported by the derived temperature, which matches that of a G4 star quite well (). Adopting a typical radius of an A5 dwarf of $1.7\mathcal{R}_\odot$ () and using the parallax of $0''.013 \pm 0''.012$ listed by , we estimate that the diameter of the secondary is unresolved at less than 0.5 mas. Therefore, we held fixed the secondary diameter at 0.2 mas in the model fit and solved for the primary diameter only (as well as the rest of the system parameters and orbital elements). This procedure is necessary because there is a correlation between the diameters and the magnitude difference related to their similar effects on measured visibilities. We note that the fitted primary diameter is consistent with the result from .

We derive $(B - V)$ colors for the individual components of $0^m95 \pm 0^m04$ and $0^m08 \pm 0^m09$ for primary and secondary, respectively (with $m_V = 4^m60$ and $m_B = 5^m38$). For this result, we extrapolated the measured magnitude difference at 500 nm to 450 nm ($\Delta m = 1^m15$) using a quadratic fit to the magnitude difference measured at $\lambda\lambda$ 800 nm, 550 nm, and 500 nm. We adopted an uncertainty of this extrapolated value of 0^m1 . The derived colors are not significantly different from values listed in for the spectral types G5III (0^m88) and A5V (0^m14).

5.7. β Trianguli

No. 111 (= 4 Tri = HR 622 = HD 13161 = SAO 55306) in B89, is the first star where we encounter a significant difference between the orbital eccentricity measured by the Mark III interferometer and that measured by using spectroscopy. The elements of the latter received a ‘b’-rating (‘good’ orbit) in B89. However, derived $e = 0.456 \pm 0.063$, much closer to our result. The differences in the spectroscopic results are attributed by Ebbighausen ‘to the non-uniform phase distribution in the earlier series, the accidental error, and the systematic differences between Yerkes and Victoria velocities’. Concerning the Mark III analysis with respect to the eccentricity, we would like to quote values derived ‘independently’ by two of the authors of this paper (MV and JTA) in 1991 with the data then available using different reduction programs: 0.46 ± 0.06 , and 0.41 ± 0.03 . This shows that the Mark III results are internally consistent, the value quoted in Table 1 being the most precise since only it was derived using the direct visibility fitting algorithm. However, only new interferometric measurements with a different instrument would allow a truly independent derivation of the orbital elements in order to verify the *accuracy* of the elements.

Until new measurements are obtained, we will resolve the issue as follows. We adopt the eccentricity from the Mark III and perform a least-squares fit of the spectroscopic elements to the data listed in . We have verified that an algorithm we wrote for this purpose derived elements almost identical to those by Ebbighausen when all elements were treated as free variables. However, parameter uncertainties we derived were somewhat larger, in particular $e = 0.53 \pm 0.03$. The increase in χ^2 for the fit with $e = 0.44$ over the model by Ebbighausen is about 20%. We derive $K_1 = (30.4 \pm 1.2)$ km/s and $K_2 = (70.3 \pm 2.8)$ km/s, compared to $K_1 = (33.3 \pm 0.9)$ km/s and $K_2 = (69.2 \pm 1.6)$ km/s obtained by Ebbighausen. With these values, we calculate (provisional) masses for the primary and secondary component of β

Trianguli of $3.7 \pm 0.4\mathcal{M}_\odot$ and $1.6 \pm 0.2\mathcal{M}_\odot$, respectively.

The results obtained in the last paragraph raise serious questions. The magnitude difference between the components is relatively small, and the color difference is negligible. Therefore, we would expect a much smaller mass ratio than was actually derived. The spectral type of the primary is A5, luminosity class III, which represents a consistent classification over the years (e.g.). The mass of the primary component seems to be too large for an A5 giant, which should be about $2 - 3\mathcal{M}_\odot$. From the evolutionary sequences calculated by S92 and S93, there is no stellar pair which comes even close the required mass ratio at the given luminosity ratio ($L_1/L_2 = 1.5$). In this context, we have to point out that there are only four radial velocity measurements which form the basis of Ebbighausen’s (1959) determination of K_2 ; did not measure the secondary spectrum since it shows only occasionally. In addition, the lines are rotationally broadened, corresponding to $v \sin i = 76\text{km/s}$ (Hoffleit & Jaschek 1982). Until reliable spectroscopic measurements are made, we refrain from tabulating the physical parameters that were derived on the basis of the currently available data.

5.8. δ Trianguli

A G0V primary dominates the spectrum of binary No. 117 (= 8 Tri = HR 660 = HD 13974 = SAO 55420) in B89, and its orbital elements were derived by . More recently, were able to measure the secondary spectrum and obtained $K_1 = 10.49 \pm 0.20$ km/s and $K_2 = 11.89 \pm 0.33$ km/s.

The orbital inclination of δ Trianguli is very difficult to measure accurately because it is close to zero. For the model given in Table 1 we fixed the angular diameters of the components at 0.6 mas and 0.3 mas for primary and secondary, respectively. These values

were derived from the $(R - I)$ color index (adopting an identical index of $(R - I) = 0^m24$ for both components) and the visual magnitudes using a method described by . With the diameters as free parameters, a least-squares fit did derive larger values (by a factor of 2), while the inclination dropped to about 163° and the magnitude differences increased slightly. However, we favor the model given in Table 1, since it is closest to the one derived by D&M with respect to the magnitude difference (D&M derived $2^m0 \pm 0^m2$), the parallax ($0''.11 \pm 0''.03$ compared to $\pi = 0''.098 \pm 0''.003$ from , and the masses ($0.6 \pm 0.4M_\odot$ and $0.5 \pm 0.3M_\odot$ compared to masses one would expect for stars very similar in type to our sun). Admittedly, the precision of our mass determination does not make this a very useful one.

From the measured magnitude differences (we extrapolate to 450 nm using a quadratic fit) we derive $(B - V)$ colors of $0^m55 \pm 0^m03$ and $1^m03 \pm 0^m08$ for primary and secondary, respectively. With bolometric corrections of -0^m08 and -0^m40 , we calculate luminosities of $(0.7 \pm 0.3)L_\odot$ and $(0.2 \pm 0.1)L_\odot$, respectively. Again, the parameters of the primary component are consistent with its classification (; according to the color, the secondary could be of type K4V ()). Unfortunately, the errors in both variables are sufficiently large as to prevent any meaningful physical discussion of δ Trianguli until better interferometric measurements are available.

6. Conclusions

We have presented the orbital elements of eight spectroscopic binaries derived from observations with the Mark III optical interferometer. The measurement of the orbital inclination provided the last piece of information necessary for the determination of component masses and luminosities of seven double-lined spectroscopic binaries. However, in two of these cases we question the spectroscopic results, since the derived physical

parameters were very much incompatible with stellar evolution models. The power of interferometric methods to resolve close binaries *and* to measure the brightness difference of the components in different wavelength bands will greatly enhance our knowledge of the fundamental physical parameters of stars if complemented by a renewed effort to detect the secondary spectra and to precisely measure the radial velocities.

We thank Lu Rarogiewicz and Craig Denison for their unfaltering support in operating the Mark III interferometer for many years. This work was supported by the Office of Naval Research. A. Q. acknowledges support by the Alexander von Humboldt foundation through a Feodor Lynen fellowship. This research has made use of the SIMBAD literature database, operated at CDS, Strasbourg, France.

References

- Abt, H. A., & Levy, S. G. 1976, *ApJS*, 30, 273
- Andersen, J. 1991, *A&A Review*, 3, 91
- Armstrong, J. T., Mozurkewich, D., Vivekanand, M., Simon, R. S., Denison, C. S.,
Johnston, K. J., Pan, X.-P., Shao, M., & Colavita, M. M. 1992, *AJ*, 104, 241
- Batten, A. H., Fisher, W. A., Fletcher, J. M., & Hill, G. 1983, *PASP*, 95, 768
- Batten, A. H., Fletcher, J. M., & MacCarthy, D. G. 1989,
Pub. Dom. Astrophys. Obs., 17, 1
- Bertelli, G., Bressan, A., Chiosi, C., Fagotto, F., & Nasi, E. 1994, *A&AS*, 106, 275
- Blackwell, D. E., Lynas-Gray, A. E., & Petford, A. D. 1991, *A&A*, 245, 567
- Cesco, C. U., & Struve, O. 1946, *ApJ*, 104, 282
- Cesco, C. U. 1946, *ApJ*, 104, 287
- Cowley, A., Cowley, C., Jaschek, M., & Jaschek, C. 1969, *AJ*, 74, 375
- Duquennoy, A., & Mayor, M. 1988, *A&A*, 195, 129
- Ebbighausen, E. G. 1959, *P.Dom.Ap.O.*, 11, 277
- Fehrenbach, Ch., & Prevot, L. 1961, *J.Obs.*, 44, 83
- Flower, P. J. 1977, *A&A*, 54, 31
- Gómez, A. E., & Abt, H. A. 1982, *PASP*, 94, 650
- Green, R. M. 1985, *Spherical Astronomy* (Cambridge University Press, Cambridge)
- Gubochkin, A. N., Miroshnichenko, A. S. 1991, *Kin. and Phys. of Cel. Bodies*, 7, 59
- Hoffleit, D., & Jaschek, C. 1982, *The Bright Star Catalogue*
(Yale University Observatory, New Haven)
- Hummel, C. A., & Armstrong, J. T. 1994, in: *Very High Angular Resolution Imaging*,
ed. by J. G. Robertson and W.J. Tango (Kluwer, Dordrecht), p.410

- Hummel, C. A., Armstrong, J. T., Quirrenbach, A., Buscher, D. F., Mozurkewich, D.,
Simon, R. S., & Johnston, K. J. 1993, *AJ*, 106, 2486
- Johansen, K. T. 1971, *A&A*, 12, 165
- Johnson, H. L., Mitchell, R. I., Iriarte, B., & Wiśniewski, W. Z. 1966,
Comm. Lunar Planetary Lab., 4, 99
- Luyten, W. J. 1936, *ApJ*, 84, 85
- Malagnini, M. L., & Morossi, C. 1990, in: *Astrophysical Ages and Dating Methods*,
ed. by É. Vangioni-Flam, M. Cassé, J. Audouze, and J. Tran Than Van
(Éditions Frontières, Gif sur Yvette), p.127
- Mozurkewich, D., Johnston, K. J., Simon, R. S., Bowers, P. F., Gaume, R. A.,
Hutter, D. J., Colavita, M. M., Shao, M., & Pan, X.P. 1991, *AJ*, 101, 2207
- Murphy, R.E. 1969, *AJ*, 74, 1082
- Nordström, B., & Johansen, K. T. 1994, *A&A*, 291, 777
- Parsons, S. B. 1983, *ApJS*, 53, 553
- Pearce, J. A. 1936, *PASP*, 48, 215
- Pease, F. G. 1927, *PASP*, 39, 313
- Petrie, R. M. 1939, *Publ. Dom. Astrophys. Obs.*, 7, 205
- Petrie, R. M. 1950, *Publ. Dom. Astrophys. Obs.*, 8, 319
- Schaerer, D., Meynet, G., Maeder, A., & Schaller, G. 1993, *A&AS*, 98, 523
- Schaller, G., Schaerer, D., Meynet, G., & Maeder, A. 1992, *A&AS*, 96, 269
- Schmidt-Kaler, T. H. 1982, *Physical Parameters of the Stars*, in: *Landolt-Bornstein*
New Series, Vol. 2b, ed. by K. Schaifers and H. H. Voigt (Springer Verlag, New York)
- Shao, M., Colavita, M. M., Hines, B. E., Staelin, D. H., Hutter, D. J.,
Johnston, K. J., Mozurkewich, D., Simon, R. S., Hershey, J. L., Hughes, J. A.,
& Kaplan, G. H. 1988, *A&A*, 193, 357
- Smalley, B., & Dworetzky, M. M. 1995, *A&A*, 293, 446

Smith, B. 1948, ApJ, 108, 504

Strassmeier, K. G., Weichinger, S., & Hanslmeier, A. 1986, Inf. Bull. Var. Stars, 2937

Struve, O., & Pogo, A. 1928, ApJ, 67, 336

Van Altena, W. F., J. T.-l. Lee, & Hoffleit, E. D. 1991, The General
Catalogue of Trigonometric Stellar Parallaxes: a preliminary version
(Yale University Observatory, New Haven)

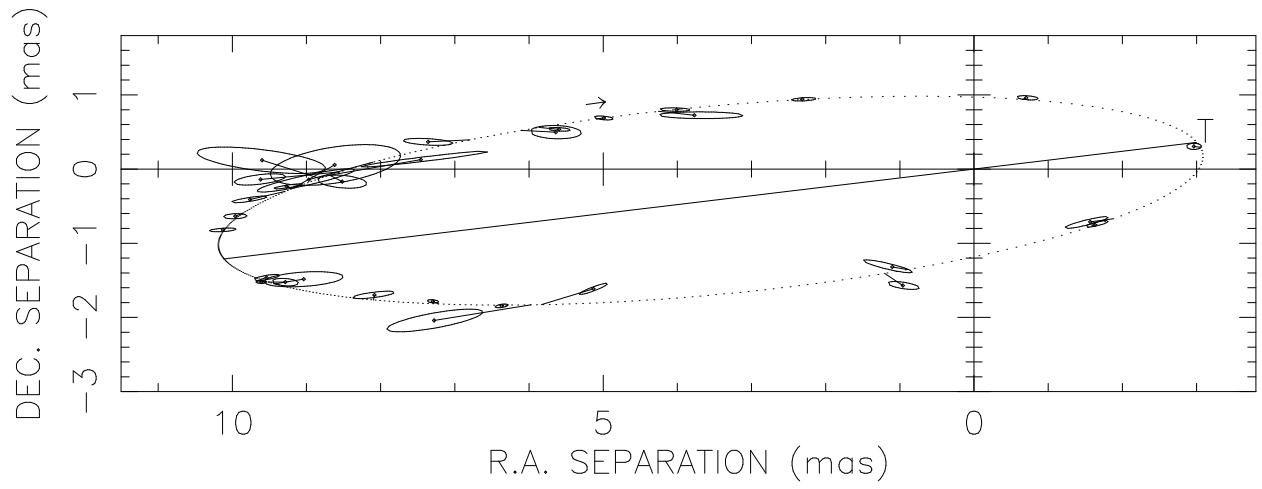


Fig. 1.— Orbit of π Andromedae.

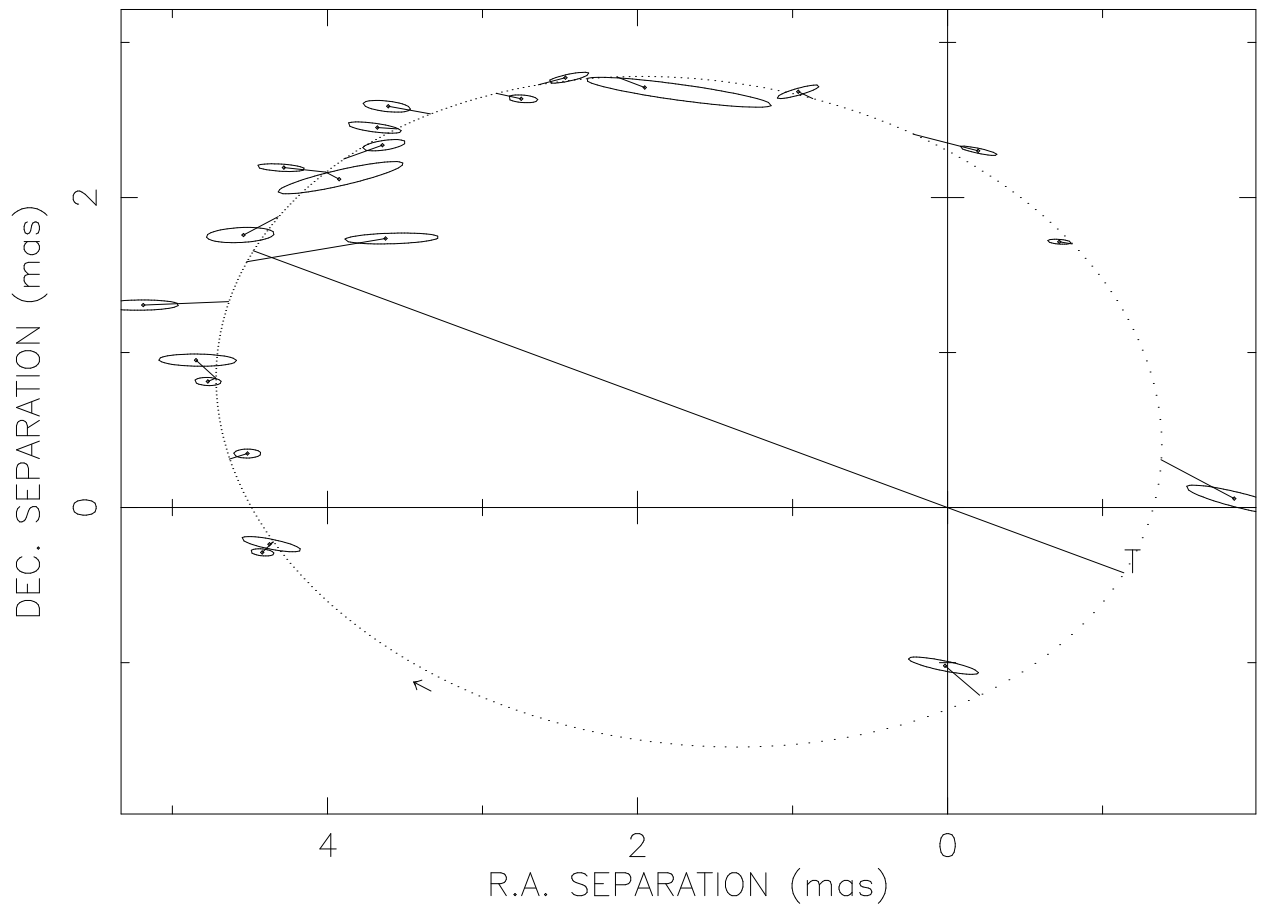


Fig. 2.— Orbit of θ Aquilae.

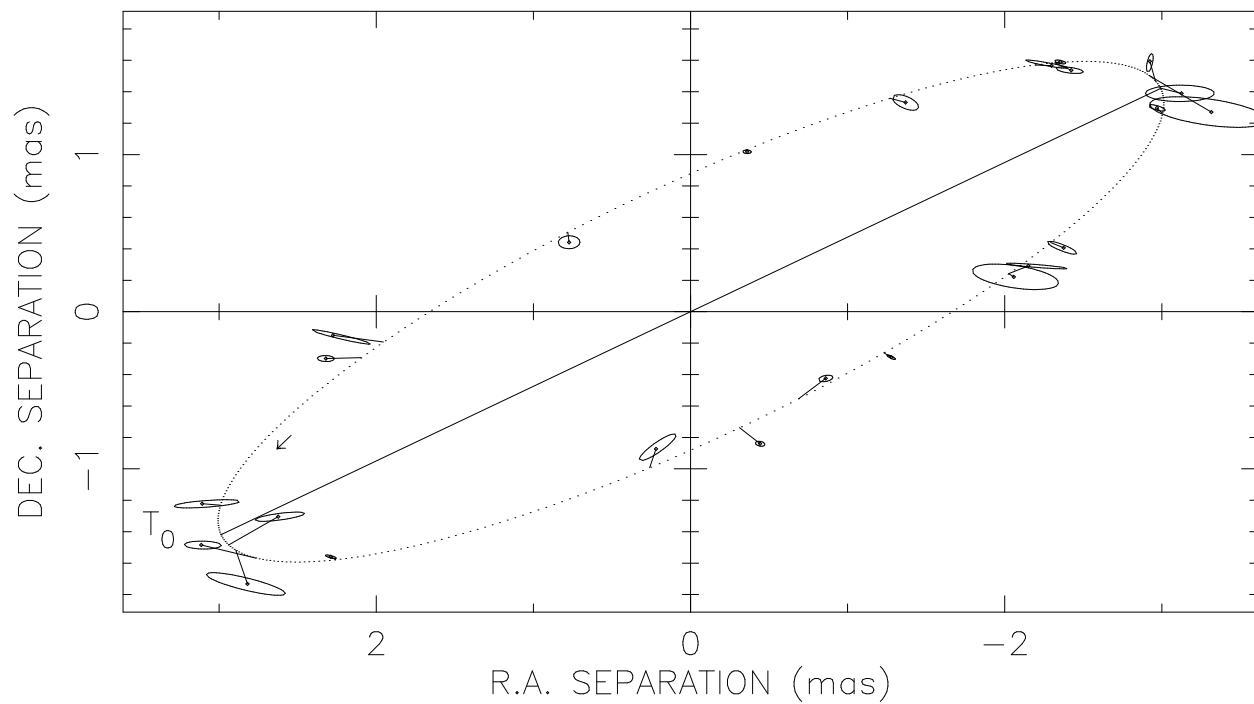


Fig. 3.— Orbit of β Aurigae.

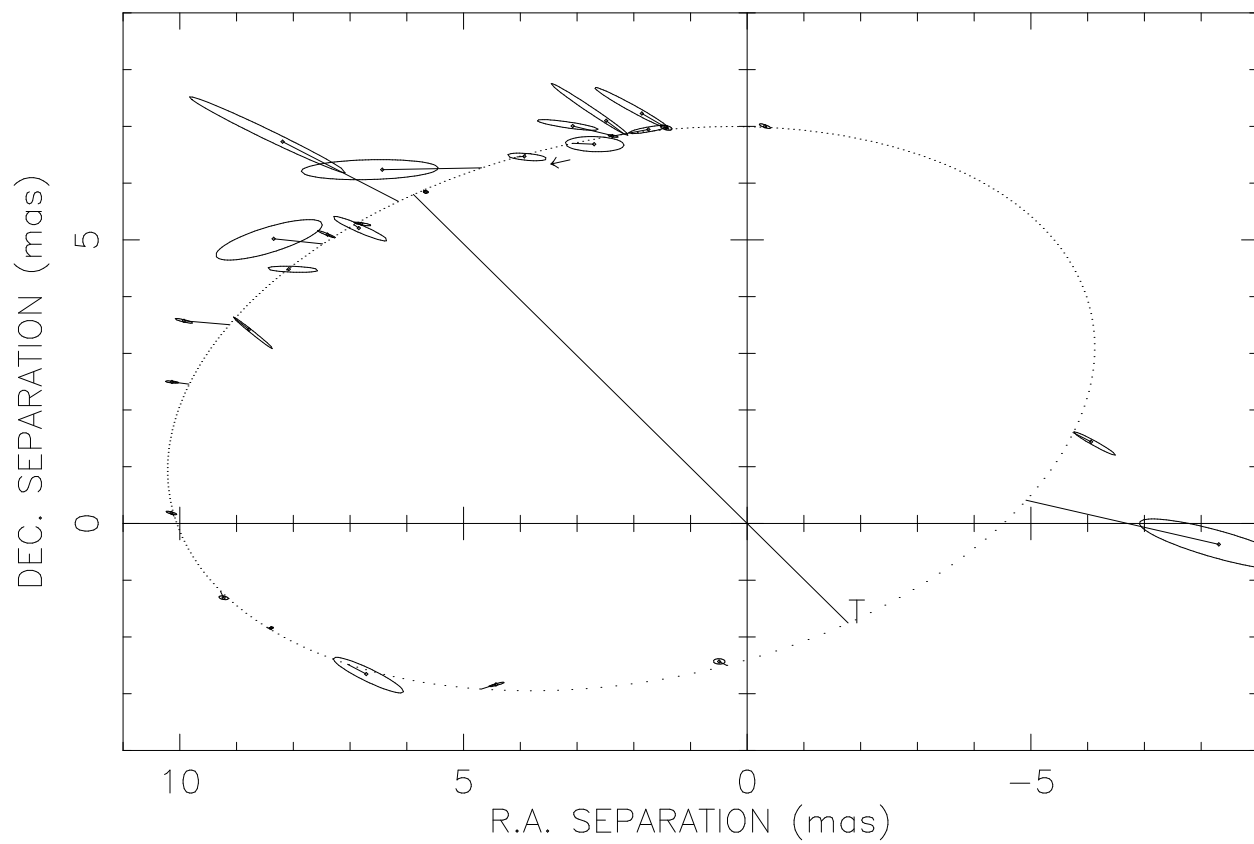


Fig. 4.— Orbit of ζ^1 Ursae Majoris.

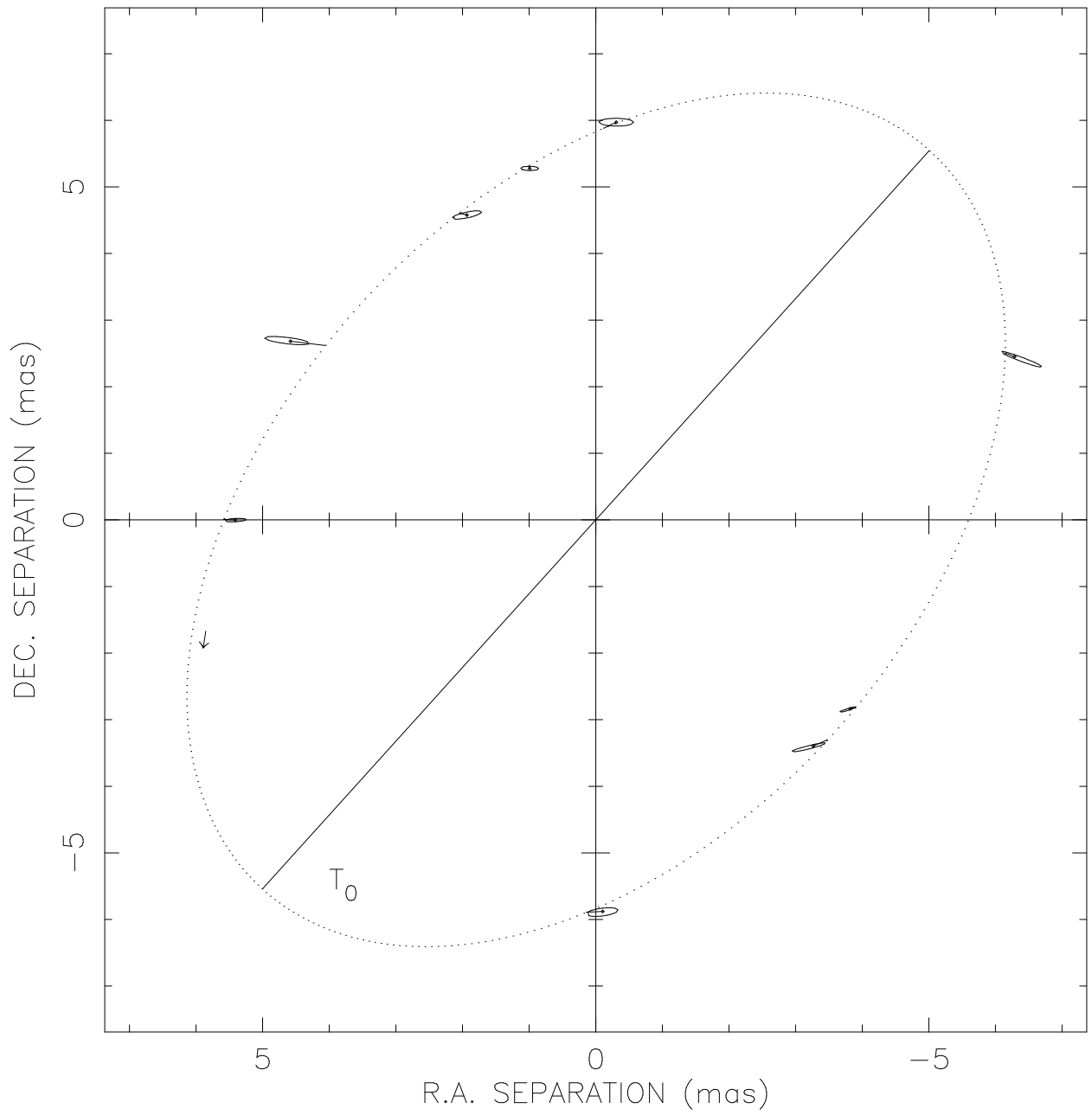


Fig. 5.— Orbit of 93 Leonis.

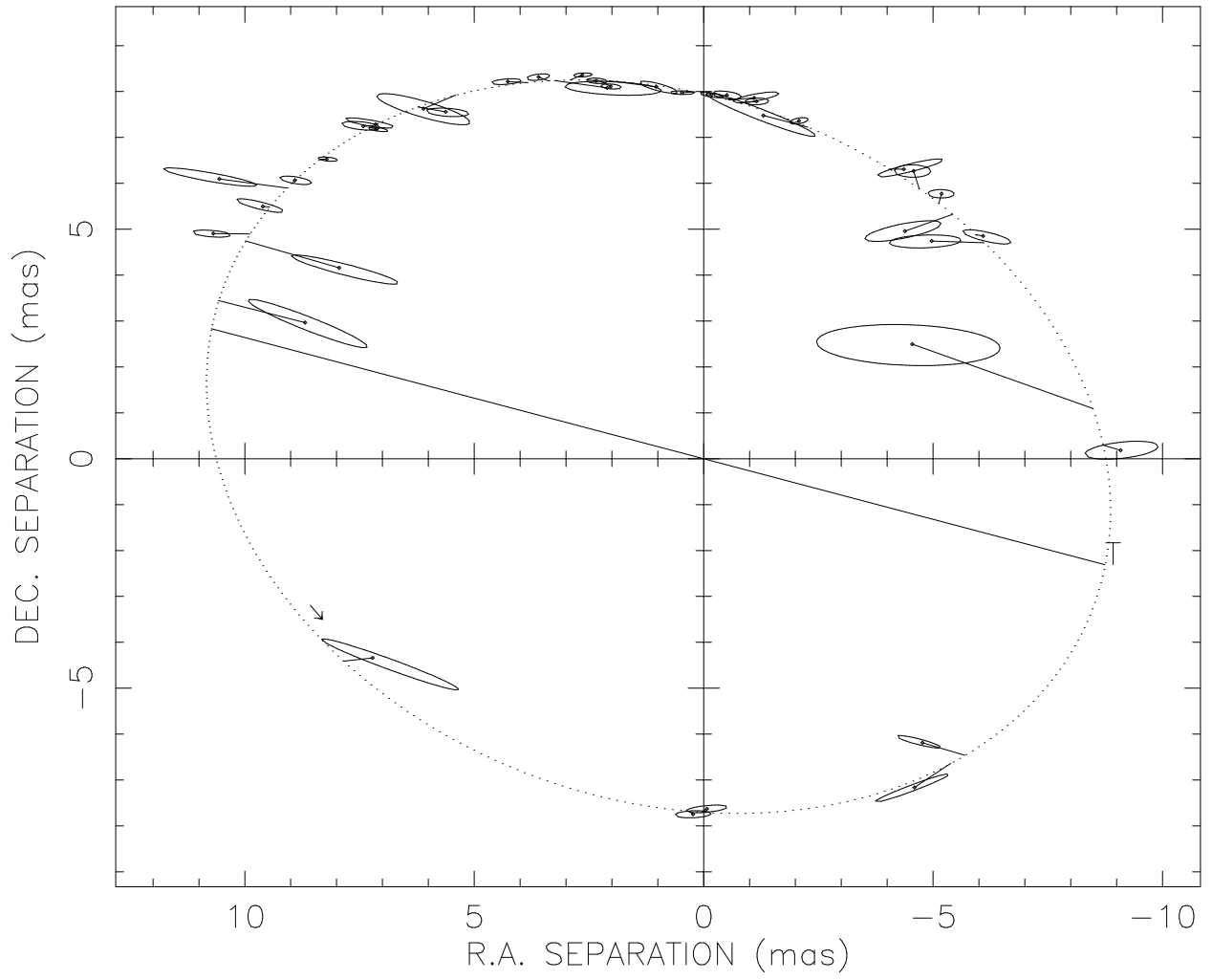


Fig. 6.— Orbit of 113 Herculis.

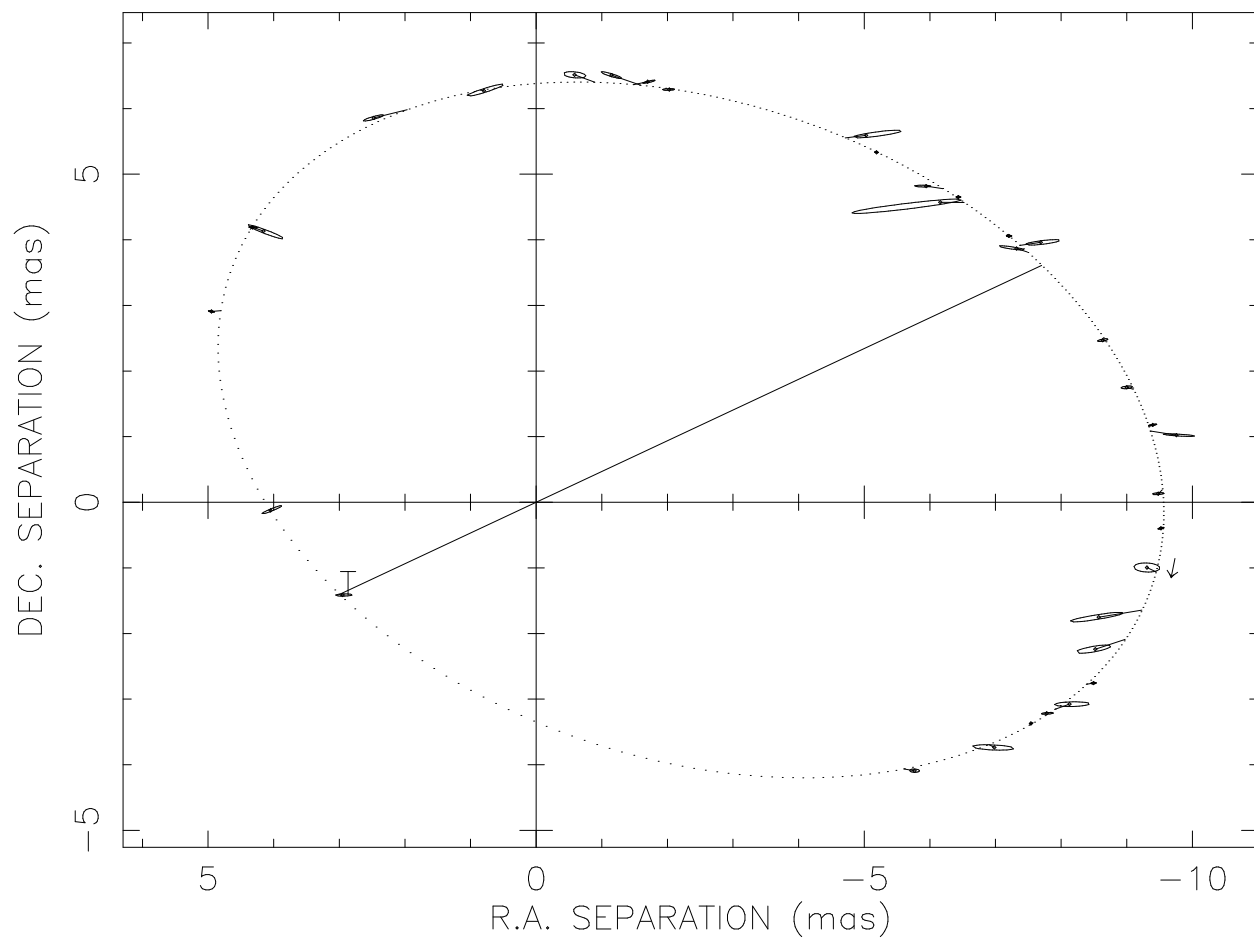


Fig. 7.— Orbit of β Trianguli.

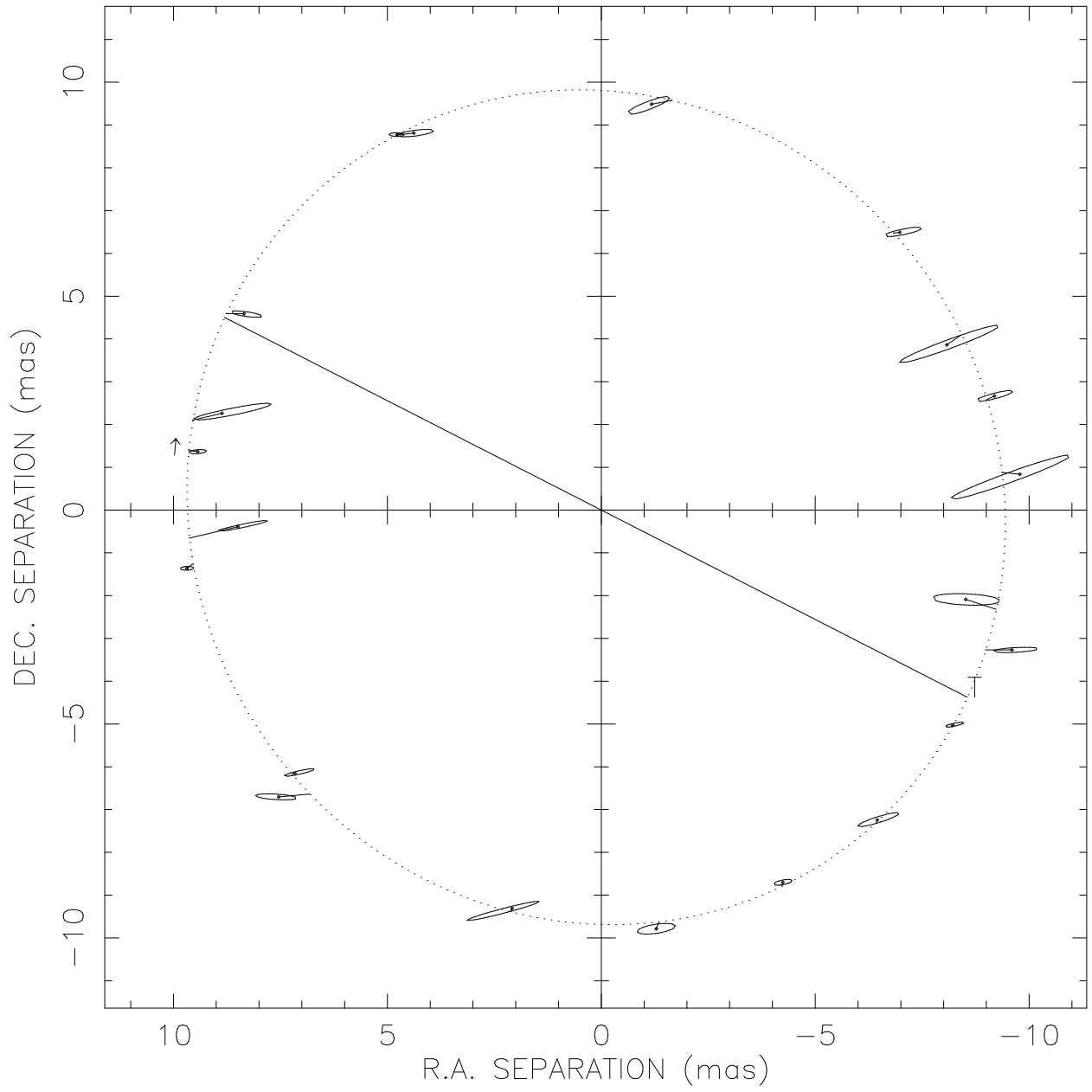


Fig. 8.— Orbit of δ Trianguli.

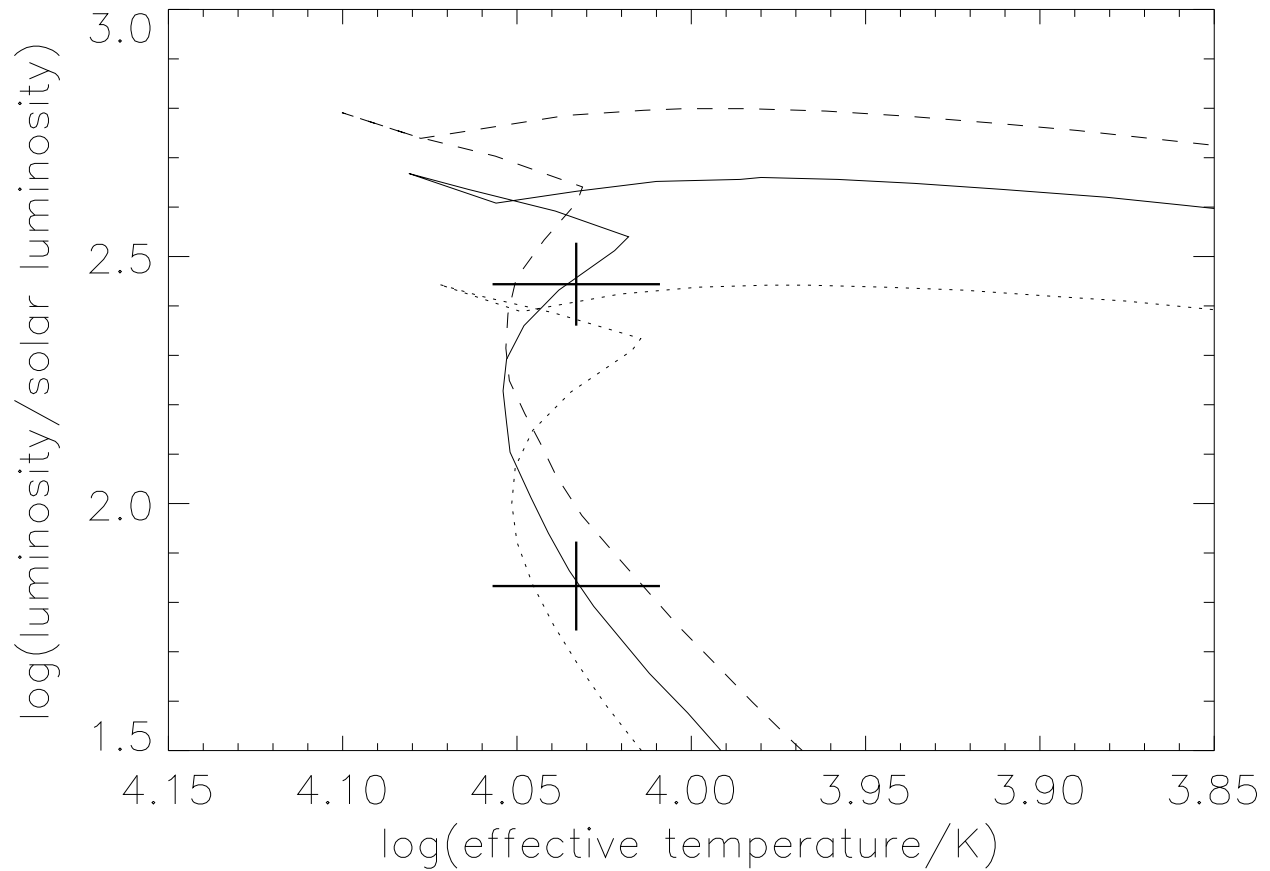


Fig. 9.— Evolutionary state of the θ Aquilae stars. Solid curve is solar-metallicity isochrone at $\log(\text{age}/\text{yr}) = 8.30$. Dashed isochrone is for $Z = 0.05$ ($\log(\text{age}/\text{yr}) = 8.16$), and dotted isochrone for $Z = 0.008$ ($\log(\text{age}/\text{yr}) = 8.45$).

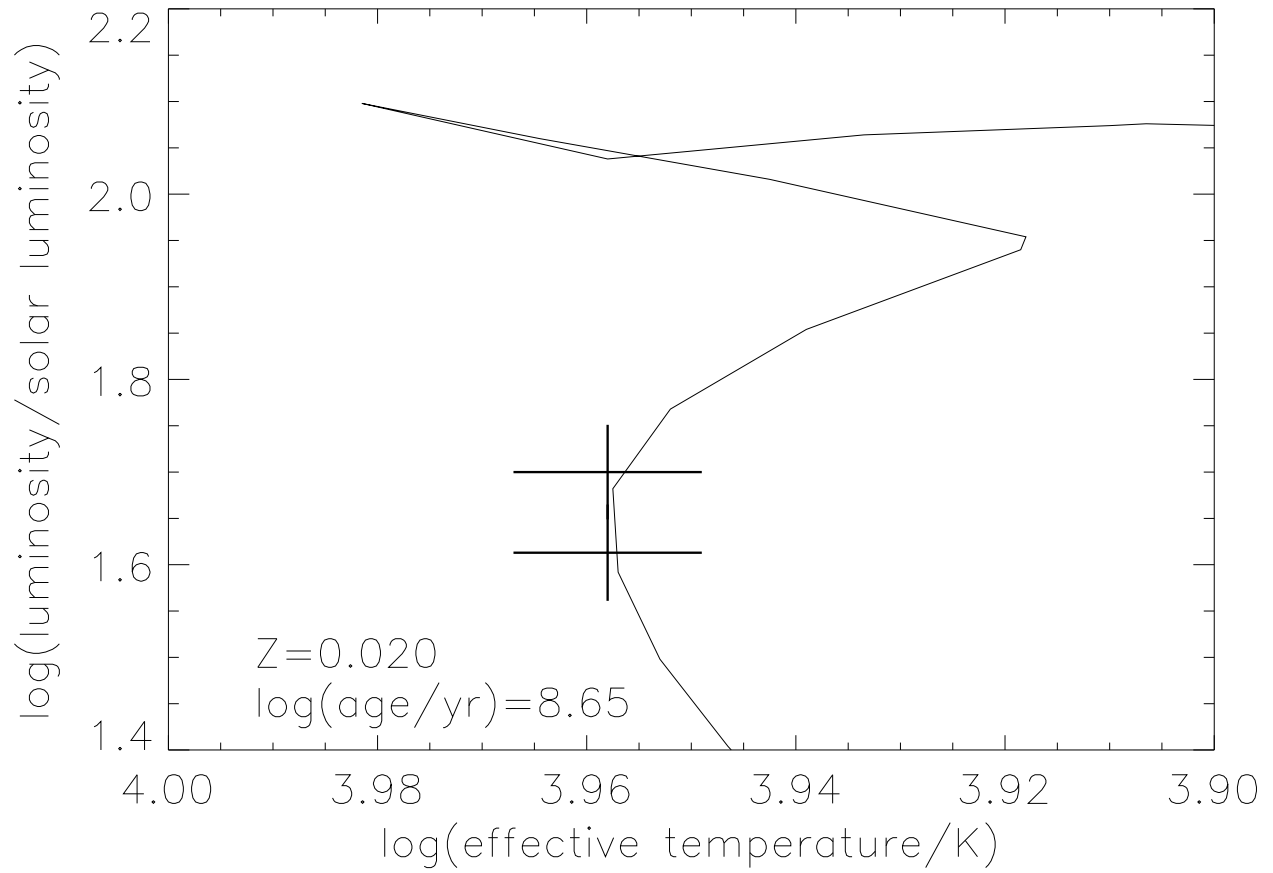


Fig. 10.— Evolutionary state of the β Aurigae stars. Solid curve is isochrone.

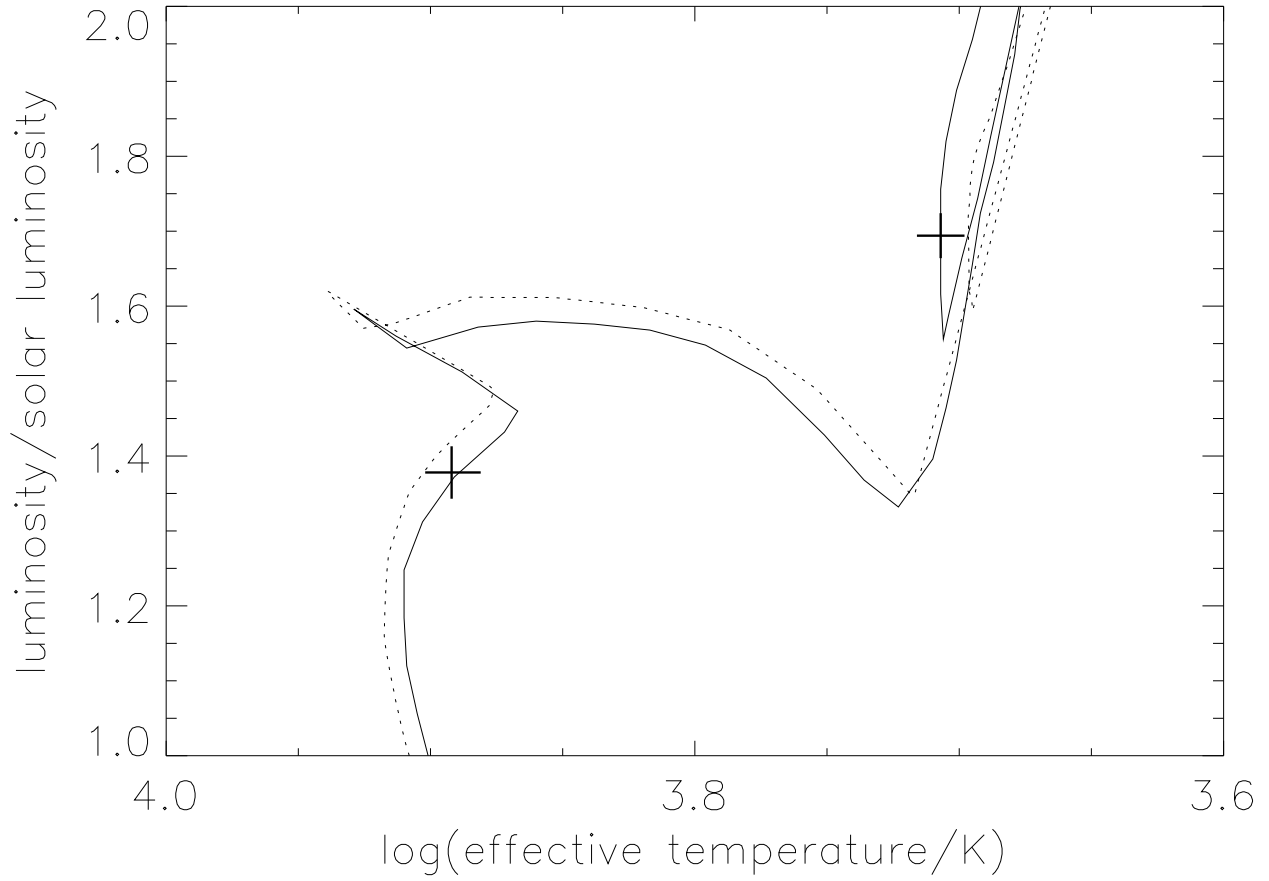


Fig. 11.— Evolutionary state of the 93 Leonis stars at $\log(\text{age}/\text{yr}) = 9.0$. Solid curve is isochrone from B94; dashed isochrone is from S93.

Table 1: Orbital elements and component parameters

	π Andromedae	θ Aquilae	β Aurigae	ζ^1 Ursae Majoris
a/mas	6.69 ± 0.05	3.2 ± 0.1	3.3 ± 0.1	9.64 ± 0.05
e_M	0.542 ± 0.006	0.60 ± 0.02	0.00 ± 0.01	0.536 ± 0.004
e_S	0.562 ± 0.007	0.607 ± 0.011	0 (fixed)	0.537 ± 0.004
$\omega_M/^\circ$	170.7 ± 0.7	215 ± 10	0 (fixed)	105.9 ± 0.3
$\omega_S/^\circ$	169.0 ± 1.0	214.5 ± 2.3	0 (fixed)	104.2 ± 1.1
$i/^\circ$	103.0 ± 0.2	143.5 ± 3.0	76.0 ± 0.4	59.7 ± 0.2
$\Omega/^\circ$ (J2000.0)	94.7 ± 0.2	99 ± 5	115.4 ± 0.5	105.9 ± 0.4
T_M (JD-244E4)	7717.7 ± 0.4	7801.7 ± 0.1	7438.65 ± 0.01^a	7636.23 ± 0.02
T_S (JD-244E4)	7716.3	7801.6	7438.48 ^a	7636.21
P_M/days	143.53 ± 0.06	17.122 ± 0.001	3.9600 ± 0.0001	20.5377 ± 0.0003
P_S/days	143.6065	17.1243	3.9600	20.53860
D_1/mas	<1	<1	1.0 ^b	0.8 ^c
D_2/mas	<1	<1	1.0 ^b	0.8 ^c
$\Delta m_{800\text{nm}}^d$	$0^m3 \pm 0^m2$	$1^m59 \pm 0^m03$	$0^m4 \pm 0^m2$	0^3
$\Delta m_{550\text{nm}}$	$0^m4 \pm 0^m1$	$1^m53 \pm 0^m05$	$0^m2 \pm 0^m2$	0^3
$\Delta m_{450\text{nm}}$	$0^m4 \pm 0^m2$	$1^m52 \pm 0^m07$	$0^m1 \pm 0^m2$	0^3
# of visibilities	1050	1047	1299	726
Mean epoch	1990.8	1991.8	1990.7	1990.6
χ_ν^2	1.1	1.9	2.3	1.8
Spec. reference	1	2	3	4

^aEpoch of passage through ascending node

^bAdopted from

^cAdopted (see text)

^d $\Delta m \equiv m_2 - m_1$

References. — (1) Pearce 1936; (2) Cesco & Struve 1946; (3) Smith 1948; (4) Fehrenbach & Prevot 1961

Table 1: Orbital elements and component parameters (continued)

	93 Leonis	113 Herculis	β Trianguli	δ Trianguli
a/mas	7.5 ± 0.1	10.1 ± 0.1	8.02 ± 0.05	9.80 ± 0.06
e_M	0 (fixed)	0.102 ± 0.005	0.440 ± 0.002	0.020 ± 0.005
e_S	0 (fixed)	0.12 ± 0.01	0.53 ± 0.02	0 (fixed)
$\omega_M/^\circ$	0 (fixed)	186.7 ± 2.0	298.1 ± 0.2	121 ± 11
$\omega_S/^\circ$	0 (fixed)	177.5 ± 5.0	318.4 ± 2.1	121 (fixed)
$i/^\circ$	50.1 ± 0.5	40.2 ± 0.6	129.9 ± 0.2	167 ± 3
$\Omega/^\circ$ (J2000.0)	138 ± 1	70.1 ± 1.2	64.9 ± 0.3	15 ± 9
T_M (JD-244E4)	7642.6 ± 0.2^a	7784.1 ± 0.8	7729.07 ± 0.03	8117.0 ± 0.2
T_S (JD-244E4)	7642.7^a	7771.6	7729.84	8118.1
P_M/days	71.69 (fixed)	245.52 ± 0.08	31.387 ± 0.001	10.0200 ± 0.0001
P_S/days	71.6900	245.3	31.3884	10.02008
D_1/mas	1.1 ± 0.2	1.4 ± 0.2	<1	<1
D_2/mas	<1	<0.5	<1	<1
$\Delta m_{800\text{nm}}^b$	$1^m14 \pm 0^m03$	$3^m00 \pm 0^m05$	$0^m51 \pm 0^m02$	$1^m64 \pm 0^m05$
$\Delta m_{550\text{nm}}$	$0^m5 \pm 0^m1$	$2^m01 \pm 0^m05$	$0^m43 \pm 0^m02$	$1^m93 \pm 0^m10$
$\Delta m_{500\text{nm}}$		$1^m61 \pm 0^m05$		$2^m14 \pm 0^m15$
$\Delta m_{450\text{nm}}$	$-0^m2 \pm 0^m2$		$0^m42 \pm 0^m04$	
# of visibilities	309	1596	1098	897
Mean epoch	1991.0	1991.3	1990.1	1992.1
χ_ν^2	1.1	1.4	1.4	1.6
Spec. Reference	1	2	3	4

^aEpoch of passage through ascending node

^b $\Delta m \equiv m_2 - m_1$

References. — (1) Batten et al. 1983; (2) Parsons 1983; (3) Ebbighausen 1959; (4) Duquennoy & Mayor 1988

Table 2: Observation and result log for π Andromedae

UT Date	Bess. Yr. (-1900)	BL [m]	No. scans	ρ [mas]	θ [deg]	σ_{maj} [mas]	σ_{min} [mas]	φ [deg]	O-C [mas]
(1)	(2)	(3)	(4)	(5)	(6)	(7)	(8)	(9)	(10)
1989									
Aug 16	89.6241	15.2	9	7.56	105.66	0.65	0.10	100.2	1.32
Sep 8	89.6871	23.6	6	9.16	99.33	0.53	0.10	93.7	0.40
Sep 9	89.6899	23.6	9	9.41	99.32	0.18	0.05	86.1	0.23
Oct 6	89.7638	31.5	8	9.98	93.65	0.16	0.03	92.2	0.11
Oct 14	89.7857	8.2	13	8.62	89.63	0.89	0.24	98.7	0.64
Oct 17	89.7939	11.4	8	9.60	89.29	0.87	0.14	83.0	0.81
Oct 18	89.7966	11.4	12	8.52	91.14	0.33	0.08	85.5	0.19
Oct 19	89.7994	15.2	5	9.62	90.83	0.35	0.06	96.8	1.07
Nov 1	89.8350	15.2	11	5.66	84.95	0.34	0.09	88.3	0.47
Nov 2	89.8377	27.0	7	5.62	84.53	0.15	0.02	86.7	0.27
Nov 5	89.8459	27.6	13	5.04	82.14	0.13	0.02	84.7	0.10
1990									
Jul 27	90.5687	31.5	8	9.77	92.40	0.24	0.03	98.8	0.48
Jul 28	90.5715	31.5	9	9.27	91.44	0.20	0.02	98.5	0.08
Aug 1	90.5824	27.0	7	7.46	89.03	0.87	0.03	96.9	1.26
Aug 5	90.5934	15.2	9	8.97	90.91	0.67	0.07	102.3	0.89
Aug 12	90.6125	23.6	10	7.37	87.15	0.33	0.04	86.9	0.57
Aug 22	90.6399	27.6	11	3.84	79.10	0.56	0.05	89.8	0.49
Aug 23	90.6426	31.5	13	4.09	78.69	0.21	0.02	88.9	0.06
Aug 28	90.6563	27.0	16	2.50	67.89	0.17	0.02	93.2	0.00
Sep 5	90.6782	15.4	27	1.19	323.86	0.14	0.03	85.9	0.06
Sep 14	90.7029	15.4	22	2.98	275.89	0.10	0.04	90.2	0.08
Oct 27	90.8206	31.5	10	7.51	103.73	0.08	0.02	85.2	0.08
1991									
Aug 3	91.5872	31.5	6	5.38	107.47	0.20	0.03	110.8	0.73
Aug 28	91.6557	31.5	8	9.73	99.01	0.07	0.02	89.2	0.06
Aug 29	91.6584	23.6	9	9.65	98.71	0.18	0.03	99.9	0.09
Sep 18	91.7132	27.0	7	10.16	94.63	0.18	0.02	93.8	0.01
Dec 6	91.9295	19.7	11	1.72	140.15	0.34	0.04	76.6	0.21
Dec 7	91.9322	15.2	12	1.84	148.53	0.22	0.04	81.5	0.30
1992									
Sep 9	92.6906	23.6	8	1.72	245.59	0.30	0.03	103.9	0.30
Sep 10	92.6933	23.6	17	1.79	245.29	0.16	0.03	103.2	0.05
Oct 9	92.7727	23.6	18	6.63	106.15	0.09	0.02	98.9	0.03
Oct 19	92.8001	23.6	8	8.26	101.85	0.28	0.04	97.1	0.07

Table 3: Observation and result log for θ Aquilae

UT Date	Bess. Yr. (-1900)	BL [m]	No. scans	ρ [mas]	θ [deg]	σ_{maj} [mas]	σ_{min} [mas]	φ [deg]	O-C [mas]
(1)	(2)	(3)	(4)	(5)	(6)	(7)	(8)	(9)	(10)
1990									
Jul 30	90.5769	27.0	10	4.33	57.33	0.14	0.03	98.2	0.27
Aug 1	90.5824	27.0	11	3.71	41.64	0.14	0.02	101.8	0.18
Aug 28	90.6563	27.0	11	4.43	93.74	0.08	0.02	84.1	0.10
Aug 30	90.6618	23.3	12	4.94	78.90	0.25	0.04	89.2	0.17
Aug 31	90.6646	23.3	13	5.35	75.87	0.25	0.03	90.5	0.55
Sep 2	90.6700	19.4	15	4.81	62.88	0.16	0.02	86.6	0.27
1991									
Aug 9	91.6037	27.0	12	4.02	64.42	0.30	0.03	91.6	0.91
1992									
Jun 30	92.4962	27.0	14	4.87	68.84	0.22	0.05	92.8	0.25
Jul 2	92.5017	27.0	16	4.44	54.34	0.15	0.03	83.7	0.28
Jul 5	92.5099	27.0	14	2.85	19.76	0.14	0.02	105.8	0.10
Jul 30	92.5784	27.0	18	4.38	93.09	0.19	0.03	78.8	0.03
Jul 31	92.5811	27.0	20	4.53	85.59	0.09	0.03	90.5	0.12
Aug 1	92.5838	27.0	26	4.84	80.33	0.09	0.03	87.8	0.05
Aug 4	92.5920	27.0	6	4.46	61.65	0.41	0.05	102.8	0.10
Aug 22	92.6413	23.1	17	4.42	56.32	0.18	0.03	82.3	0.12
Aug 23	92.6441	23.1	22	3.81	46.21	0.10	0.02	85.8	0.16
Aug 24	92.6468	23.1	16	3.34	35.80	0.60	0.05	82.2	0.19
Aug 26	92.6523	23.1	20	2.31	-4.88	0.13	0.02	78.2	0.43
Aug 27	92.6550	23.1	23	1.86	337.21	0.08	0.01	85.7	0.08
Aug 28	92.6578	23.1	22	1.85	271.79	0.35	0.05	76.0	0.54
Aug 29	92.6605	23.1	24	1.02	179.04	0.23	0.03	78.4	0.29

Table 4: Observation and result log for β Aurigae

UT Date	Bess. Yr. (-1900)	BL [m]	No. scans	ρ [mas]	θ [deg]	σ_{maj} [mas]	σ_{min} [mas]	φ [deg]	O-C [mas]
(1)	(2)	(3)	(4)	(5)	(6)	(7)	(8)	(9)	(10)
1988									
Oct 4	88.7590	19.1	11	3.45	295.50	0.12	0.03	89.1	0.36
Oct 22	88.8083	23.1	8	2.87	122.39	0.09	0.02	83.0	0.12
Oct 23	88.8110	23.1	10	2.28	273.78	0.19	0.01	76.7	0.31
Oct 24	88.8137	27.6	13	2.77	304.27	0.04	0.01	75.9	0.05
Oct 25	88.8165	31.5	5	2.17	97.71	0.20	0.01	85.5	0.12
Oct 26	88.8192	31.5	3	2.78	124.28	0.14	0.01	79.7	0.12
1989									
Oct 27	89.8213	15.2	4	3.31	301.57	0.26	0.04	76.3	0.23
Nov 5	89.8459	27.6	22	1.31	77.24	0.03	0.01	64.8	0.05
Dec 3	89.9226	15.4	19	2.41	99.73	0.10	0.02	68.5	0.08
1991									
Oct 21	91.8035	19.7	16	2.34	277.32	0.05	0.02	88.4	0.21
Nov 13	91.8665	11.4	31	1.91	134.21	0.09	0.04	67.0	0.12
Dec 3	91.9212	27.6	18	1.08	160.51	0.03	0.01	88.2	0.02
Dec 4	91.9240	27.6	10	3.34	291.47	0.21	0.02	94.2	0.11
Dec 5	91.9267	23.6	8	0.90	345.91	0.14	0.03	125.0	0.11
Dec 6	91.9295	19.7	25	3.24	113.60	0.05	0.01	73.5	0.05
1992									
Oct 9	92.7727	23.6	15	0.95	27.82	0.03	0.01	79.7	0.16
Oct 10	92.7755	12.0	20	3.42	113.98	0.22	0.05	90.1	0.14
Oct 14	92.7864	12.0	30	3.33	118.60	0.06	0.02	167.4	0.13
Oct 16	92.7919	23.6	9	2.93	296.44	0.16	0.02	97.5	0.36
Oct 17	92.7946	23.6	15	0.96	63.74	0.05	0.02	101.2	0.20
Oct 18	92.7974	12.0	18	3.55	110.98	0.38	0.08	82.0	0.46
Oct 19	92.8001	23.6	15	0.89	240.22	0.07	0.04	92.1	0.06
Nov 15	92.8740	27.6	15	2.84	124.04	0.04	0.01	78.4	0.05
Nov 18	92.8823	12.0	20	2.07	96.16	0.28	0.07	81.6	0.03

Table 5: Observation and result log for ζ^1 Ursae Majoris

UT Date	Bess. Yr.	BL [m]	No. scans	ρ [mas]	θ [deg]	σ_{maj} [mas]	σ_{min} [mas]	φ [deg]	O-C [mas]
(1)	(-1900) (2)	(3)	(4)	(5)	(6)	(7)	(8)	(9)	(10)
1989									
Apr 9	89.2710	15.2	18	8.14	44.11	0.05	0.02	81.3	0.05
Apr 16	89.2901	19.7	12	9.32	98.07	0.08	0.03	80.4	0.12
Apr 18	89.2956	19.7	6	5.26	122.63	0.14	0.02	105.1	0.28
May 18	89.3777	23.6	18	7.23	19.19	0.09	0.01	81.4	0.04
May 19	89.3805	23.6	16	7.57	31.27	0.34	0.06	84.9	0.13
Jul 18	89.5447	5.3	4	7.46	14.42	0.74	0.06	61.2	0.55
Jul 21	89.5530	6.9	3	10.60	50.58	1.53	0.09	64.2	2.29
Aug 8	89.6022	8.2	4	7.52	19.30	0.82	0.05	56.2	0.40
Aug 13	89.6159	11.4	3	9.42	68.72	0.45	0.03	231.3	0.32
1990									
Mar 22	90.2210	15.2	3	7.16	14.07	0.35	0.04	100.0	0.58
Mar 25	90.2292	11.4	9	8.61	52.18	0.15	0.02	80.4	0.10
Mar 26	90.2320	11.4	6	9.24	60.99	0.45	0.05	88.0	0.04
Apr 10	90.2730	8.2	8	7.01	357.45	0.10	0.02	70.9	0.03
Apr 11	90.2758	8.2	6	7.12	11.55	0.10	0.04	75.5	0.04
Apr 12	90.2785	4.3	10	7.21	21.98	0.52	0.13	88.4	0.38
Apr 13	90.2812	4.3	7	8.96	45.89	1.21	0.17	91.4	1.75
Apr 15	90.2867	3.0	11	9.74	58.98	0.98	0.22	106.9	0.87
Jun 2	90.4181	5.3	4	7.22	111.55	0.69	0.11	64.3	0.37
Jun 5	90.4264	6.9	7	8.32	267.46	1.43	0.24	74.4	3.49
Jun 26	90.4838	11.4	4	6.23	283.38	0.42	0.04	61.1	0.36
Jul 6	90.5112	23.6	5	8.98	55.47	0.17	0.02	68.3	0.11
1992									
Feb 28	92.1594	19.7	11	8.59	102.38	0.04	0.01	103.1	0.07
May 2	92.3347	11.4	21	2.48	168.51	0.10	0.05	87.8	0.15
May 31	92.4141	19.7	5	7.65	23.70	0.54	0.05	81.7	0.74
Jun 3	92.4223	19.7	9	8.60	52.74	0.52	0.07	66.6	0.11
Jun 5	92.4278	19.7	8	10.55	70.21	0.16	0.02	76.7	0.79
Jun 6	92.4305	19.7	10	10.44	76.18	0.12	0.02	84.1	0.30
Jun 8	92.4360	19.7	14	10.15	88.95	0.10	0.02	75.4	0.07

Table 6: Observation and result log for 93 Leonis

UT Date (1)	Bess. Yr. (-1900) (2)	BL [m] (3)	No. scans (4)	ρ [mas] (5)	θ [deg] (6)	σ_{maj} [mas] (7)	σ_{min} [mas] (8)	φ [deg] (9)	O-C [mas] (10)
1989									
Apr 9	89.2710	15.2	12	5.31	59.66	0.34	0.05	83.2	0.53
1990									
Mar 7	90.1799	31.5	10	6.75	291.30	0.33	0.03	69.6	0.16
Mar 25	90.2292	11.4	7	5.98	357.04	0.26	0.06	89.5	0.22
Dec 8	90.9356	31.5	7	4.71	223.87	0.26	0.02	104.1	0.24
Dec 9	90.9383	31.5	16	4.76	233.41	0.12	0.01	107.2	0.09
1991									
Jan 19	91.0506	31.5	9	5.41	90.03	0.16	0.02	93.1	0.18
1992									
Feb 4	92.0937	27.0	14	5.88	181.03	0.24	0.06	97.2	0.25
Mar 13	92.1978	27.0	12	5.37	10.63	0.13	0.03	89.0	0.04
Mar 15	92.2033	27.0	16	4.97	22.89	0.22	0.04	101.8	0.12

Table 7: Observation and result log for 113 Herculis

UT Date (1)	Bess. Yr. (-1900) (2)	BL [m] (3)	No. scans (4)	ρ [mas] (5)	θ [deg] (6)	σ_{maj} [mas] (7)	σ_{min} [mas] (8)	φ [deg] (9)	O-C [mas] (10)
1990									
Jun 2	90.4181	5.3	7	5.19	298.75	2.00	0.44	88.0	4.17
Jun 23	90.4756	8.2	9	6.62	318.53	0.84	0.16	101.3	1.10
Jul 7	90.5140	23.6	4	7.59	350.13	1.28	0.12	68.8	1.00
Jul 8	90.5167	23.6	13	7.65	344.24	0.20	0.06	99.8	0.07
Jul 13	90.5304	27.6	9	7.87	351.56	0.26	0.07	92.1	0.37
Jul 14	90.5331	27.6	8	7.94	352.04	0.51	0.08	100.3	0.56
Jul 15	90.5359	27.6	16	7.94	356.35	0.32	0.08	82.6	0.22
Jul 16	90.5386	31.5	11	7.93	358.73	0.27	0.05	81.2	0.13
Jul 17	90.5413	31.5	11	7.99	3.38	0.27	0.04	89.4	0.26
Jul 28	90.5715	31.5	17	8.77	17.55	0.20	0.04	92.8	0.29
Jul 30	90.5769	27.0	15	9.06	23.40	0.25	0.06	97.1	0.23
Aug 1	90.5824	27.0	16	9.26	27.46	0.33	0.06	94.5	0.42
Aug 8	90.6016	15.2	9	9.77	38.69	1.06	0.17	73.8	0.76
Aug 12	90.6125	23.6	13	9.42	36.65	0.47	0.09	86.0	0.62
Aug 17	90.6262	27.6	18	10.37	45.68	0.42	0.09	84.2	0.23
Aug 24	90.6454	31.5	16	10.49	51.52	0.21	0.04	84.4	0.16
Aug 28	90.6563	27.0	8	10.78	55.75	0.35	0.07	80.9	0.05
Aug 29	90.6591	23.3	9	12.19	59.99	1.03	0.09	80.0	1.49
Sep 1	90.6673	19.4	12	11.07	60.23	0.53	0.08	76.2	0.15
Sep 5	90.6782	15.4	17	11.76	65.35	0.42	0.07	85.5	0.80
Sep 6	90.6810	15.2	12	8.97	62.36	1.20	0.12	75.7	2.12
Sep 14	90.7029	15.4	7	9.18	71.15	1.39	0.15	68.6	1.95
Oct 28	90.8233	31.5	7	8.42	121.03	1.59	0.11	69.9	0.64
1991									
Aug 3	91.5872	31.5	13	7.75	178.29	0.39	0.08	92.2	0.10
Aug 4	91.5900	31.5	17	7.63	180.51	0.45	0.07	95.4	0.14
Aug 28	91.6557	31.5	10	7.81	217.61	0.50	0.06	75.8	0.97
1992									
Apr 28	92.3237	23.6	17	8.51	212.66	0.86	0.07	110.5	0.95
Jun 4	92.4250	27.0	14	9.09	271.17	0.80	0.18	96.2	0.40
Jun 25	92.4825	31.5	20	6.87	313.68	0.78	0.14	92.0	1.15
Jun 26	92.4853	31.5	20	7.79	308.55	0.54	0.10	77.0	0.17
Jun 30	92.4962	27.0	20	7.76	318.07	0.29	0.09	89.1	0.22
Jul 2	92.5017	27.0	18	7.76	323.88	0.40	0.14	89.3	0.41
Jul 5	92.5099	27.0	12	7.67	325.32	0.74	0.09	104.0	0.32
Jul 30	92.5784	27.0	14	8.17	7.27	0.43	0.08	75.2	1.02
Jul 31	92.5811	27.0	16	8.36	14.03	0.22	0.05	85.7	0.30
Aug 1	92.5838	27.0	22	8.56	15.87	0.23	0.06	86.6	0.20
Aug 4	92.5920	27.0	7	8.35	14.59	1.05	0.14	87.4	1.16
Aug 22	92.6413	23.1	16	10.21	44.47	0.54	0.06	80.4	0.07
Aug 23	92.6441	23.1	21	10.12	44.76	0.22	0.04	82.3	0.15

Table 8: Observation and result log for β Trianguli

UT Date	Bess. Yr.	BL [m]	No. scans	ρ [mas]	θ [deg]	σ_{maj} [mas]	σ_{min} [mas]	φ [deg]	O-C [mas]
(1)	(2)	(3)	(4)	(5)	(6)	(7)	(8)	(9)	(10)
1989									
Aug 13	89.6159	11.4	3	8.75	258.46	0.41	0.04	99.1	0.67
Sep 6	89.6816	27.6	9	8.28	297.84	0.19	0.02	81.9	0.17
Sep 8	89.6871	23.6	12	8.98	285.97	0.08	0.01	100.8	0.05
Sep 9	89.6899	23.6	14	9.17	281.01	0.09	0.02	95.7	0.10
Sep 11	89.6953	19.7	11	9.49	270.79	0.09	0.01	94.2	0.08
Sep 14	89.7035	8.2	15	8.81	255.28	0.27	0.04	100.0	0.48
Sep 15	89.7063	23.1	19	8.93	252.03	0.05	0.01	93.6	0.11
Sep 22	89.7254	23.1	12	3.27	115.61	0.13	0.02	91.2	0.03
Oct 6	89.7638	31.5	11	7.94	305.86	0.04	0.01	88.7	0.02
Oct 7	89.7665	31.5	10	8.27	299.39	0.04	0.01	88.4	0.00
Oct 14	89.7857	8.2	16	9.39	263.86	0.20	0.07	87.6	0.12
Oct 17	89.7939	11.4	10	8.69	249.26	0.27	0.04	91.3	0.24
Oct 18	89.7966	11.4	11	7.92	241.85	0.32	0.04	87.5	0.10
Oct 19	89.7994	15.2	6	7.07	234.65	0.08	0.03	88.8	0.17
Oct 27	89.8213	15.2	5	5.87	45.19	0.30	0.03	69.4	0.18
Nov 1	89.8350	15.2	11	6.54	354.86	0.17	0.05	84.6	0.33
Nov 2	89.8377	27.0	7	6.61	342.12	0.09	0.01	91.2	0.01
Nov 5	89.8459	27.6	18	7.44	315.81	0.03	0.01	80.7	0.01
Dec 3	89.9226	15.4	9	6.61	350.01	0.16	0.02	73.0	0.48
Dec 9	89.9390	11.4	6	8.65	297.25	0.26	0.03	96.8	0.32
Dec 13	89.9500	19.7	6	9.81	275.99	0.24	0.01	86.7	0.41
1990									
Aug 8	90.6016	15.2	9	6.36	22.92	0.16	0.02	105.6	0.53
Aug 9	90.6043	19.7	9	6.32	7.24	0.30	0.03	107.4	0.03
Aug 11	90.6098	23.6	14	6.63	345.16	0.10	0.01	103.1	0.21
Aug 14	90.6180	23.6	11	7.56	317.75	0.29	0.03	97.6	0.38
Aug 16	90.6235	27.6	5	7.67	306.59	0.84	0.04	96.9	0.36
Aug 21	90.6372	27.6	13	9.47	277.15	0.06	0.01	99.0	0.07
Aug 23	90.6426	31.5	12	9.53	267.62	0.05	0.01	102.1	0.03
Aug 27	90.6536	27.0	11	8.42	247.54	0.09	0.01	93.7	0.02
Sep 3	90.6728	15.4	19	4.05	91.75	0.17	0.02	112.1	0.01
Sep 16	90.7084	27.0	5	7.65	309.04	0.13	0.01	89.4	0.26
Oct 29	90.8261	31.5	23	8.26	245.91	0.02	0.01	97.6	0.04
Dec 8	90.9356	31.5	7	5.74	59.56	0.05	0.01	81.1	0.14
Dec 9	90.9383	31.5	7	6.02	45.90	0.07	0.01	85.5	0.04

Table 9: Observation and result log for δ Trianguli

UT Date	Bess. Yr. (-1900)	BL [m]	No. scans	ρ [mas]	θ [deg]	σ_{maj} [mas]	σ_{min} [mas]	φ [deg]	O-C [mas]
(1)	(2)	(3)	(4)	(5)	(6)	(7)	(8)	(9)	(10)
1990									
Aug 22	90.6399	27.6	14	8.95	295.56	1.24	0.10	110.2	0.42
Aug 24	90.6454	31.5	10	9.70	221.68	0.51	0.07	107.2	0.04
Aug 28	90.6563	27.0	12	9.15	75.70	0.93	0.08	101.1	0.70
Sep 14	90.7029	15.4	16	9.87	187.47	0.45	0.11	98.3	0.18
Oct 27	90.8206	31.5	21	9.53	81.76	0.20	0.05	94.3	0.22
1991									
Aug 28	91.6557	31.5	10	9.57	286.18	0.44	0.06	104.5	0.20
Sep 18	91.7132	27.0	8	10.14	251.19	0.53	0.05	92.9	0.62
Dec 7	91.9322	15.2	10	8.77	256.22	0.79	0.13	87.6	0.75
1992									
Aug 21	92.6386	19.7	12	9.56	352.94	0.53	0.09	110.9	0.48
Aug 22	92.6413	23.1	14	9.53	312.93	0.45	0.06	101.6	0.15
Aug 23	92.6441	23.1	11	9.82	274.90	1.49	0.12	109.9	0.42
Aug 24	92.6468	23.1	15	9.63	238.54	0.22	0.03	101.9	0.03
Aug 26	92.6523	23.1	8	9.54	167.37	0.88	0.05	104.6	0.09
Aug 27	92.6550	23.1	19	9.44	130.68	0.37	0.04	102.8	0.08
Aug 28	92.6578	23.1	22	8.50	92.62	0.59	0.04	101.7	1.17
Oct 4	92.7591	23.6	13	9.68	205.99	0.22	0.05	101.1	0.09
Oct 9	92.7727	23.6	22	9.99	28.56	0.17	0.04	87.9	0.10
Oct 16	92.7919	23.6	6	10.09	131.63	0.48	0.06	86.5	0.73
Oct 17	92.7946	23.6	20	9.78	98.00	0.16	0.04	92.2	0.17
Oct 18	92.7974	12.0	22	9.53	61.20	0.37	0.05	82.1	0.42
Oct 19	92.8001	23.6	15	9.84	26.43	0.43	0.07	97.4	0.41

Table 10: Physical parameters of θ Aquilae

Parameter	Primary (B9.5III)	Secondary (B9.5III)
K [km/s]	51.0 ± 1.3	63.7 ± 1.4
$\mathcal{M}/\mathcal{M}_{\odot}$	3.6 ± 0.8	2.9 ± 0.6
D [pc]		75.4 ± 6.0
$(B - V)$		$-0^{\text{m}}07 \pm 0^{\text{m}}03$
T_{eff}/K		10800 ± 600
BC		$-0^{\text{m}}46 \pm 0^{\text{m}}12$
M_{bol}	$-1^{\text{m}}39 \pm 0^{\text{m}}21$	$0^{\text{m}}14 \pm 0^{\text{m}}22$
L/L_{\odot}	278 ± 54	68 ± 14
R/R_{\odot}	4.8 ± 0.5	2.4 ± 0.2

Table 11: Physical parameters of β Aurigae

Parameter	Primary (A2IV)	Secondary (A2IV)
K [km/s]	107.46 ± 0.58	111.49 ± 0.55
$\mathcal{M}/\mathcal{M}_{\odot}$	2.41 ± 0.03	2.32 ± 0.03
D [pc]		24.9 ± 0.5
$(B - V)$		$0^{\text{m}}03 \pm 0^{\text{m}}15$
T_{eff}/K		9070 ± 200
BC		$-0^{\text{m}}10 \pm 0^{\text{m}}05$
M_{bol}	$0^{\text{m}}48 \pm 0^{\text{m}}12$	$0^{\text{m}}68 \pm 0^{\text{m}}14$
L/L_{\odot}	50 ± 6	41 ± 5
R/R_{\odot}	2.9 ± 0.2	2.6 ± 0.2

Table 12: Physical parameters of ζ^1 Ursae Majoris

Parameter	Primary (A2V)	Secondary (A2V)
K [km/s]	68.80 ± 0.79	67.60 ± 0.91
$\mathcal{M}/\mathcal{M}_{\odot}$	2.51 ± 0.08	2.55 ± 0.07
D [pc]		26.1 ± 0.3
$(B - V)$		$0^{\text{m}}02 \pm 0^{\text{m}}08$
T_{eff}/K		9000 ± 200
BC		$-0^{\text{m}}09 \pm 0^{\text{m}}06$
M_{bol}		$0^{\text{m}}85 \pm 0^{\text{m}}08$
L/L_{\odot}		35.2 ± 2.7
R/R_{\odot}		2.5 ± 0.1

Table 13: Physical parameters of 93 Leonis

Parameter	Primary (G5III)	Secondary (A7V)
K [km/s]	29.67 ± 0.29	33.8 ± 2.1
$\mathcal{M}/\mathcal{M}_\odot$	2.25 ± 0.29	1.97 ± 0.15
D [pc]	72.7 ± 2.7	
$(B - V)$	$0^{\text{m}}9 \pm 0^{\text{m}}1$	$0^{\text{m}}2 \pm 0^{\text{m}}1$
T_{eff}/K	5100 ± 100	7800 ± 200
BC	$-0^{\text{m}}27 \pm 0^{\text{m}}05$	$0^{\text{m}}02 \pm 0^{\text{m}}05$
M_{bol}	$0^{\text{m}}48 \pm 0^{\text{m}}07$	$1^{\text{m}}27 \pm 0^{\text{m}}08$
L/L_\odot	49.4 ± 3.4	23.9 ± 1.9
R/R_\odot	9.1 ± 0.5	2.7 ± 0.2